NUREG/CR-5013
MEA-2232

Fatigue Life Characterization of Smooth and Notched Piping Steel Specimens in 288°C Air Environments

Prepared by J. B. Terrell

Materials Engineering Associates, Inc.

Prepared for
U.S. Nuclear Regulatory Commission

NOTICE

Availability of Reference Materials Cited in NRC Publications

Most documents cited in NRC publications will be available from one of the following sources:

1. The NRC Public Document Room, 1717 H Street, N.W.
   Washington, DC 20555
2. The Superintendent of Documents, U.S. Government Printing Office, Post Office Box 37082, Washington, DC 20013-7082
3. The National Technical Information Service, Springfield, VA 22161

Although the listing that follows represents the majority of documents cited in NRC publications, it is not intended to be exhaustive.

Referenced documents available for inspection and copying for a fee from the NRC Public Document Room include NRC correspondence and internal NRC memoranda; NRC Office of Inspection and Enforcement bulletins, circulars, information notices, inspection and investigation notices; Licensee Event Reports; vendor reports and correspondence; Commission papers; and applicant and licensee documents and correspondence.

The following documents in the NUREG series are available for purchase from the GPO Sales Program: formal NRC staff and contractor reports, NRC-sponsored conference proceedings, and NRC booklets and brochures. Also available are Regulatory Guides, NRC regulations in the *Code of Federal Regulations*, and *Nuclear Regulatory Commission Issuances*.

Documents available from the National Technical Information Service include NUREG series reports and technical reports prepared by other federal agencies and reports prepared by the Atomic Energy Commission, forerunner agency to the Nuclear Regulatory Commission.

Documents available from public and special technical libraries include all open literature items, such as books, journal and periodical articles, and transactions. *Federal Register* notices, federal and state legislation, and congressional reports can usually be obtained from these libraries.

Documents such as theses, dissertations, foreign reports and translations, and non-NRC conference proceedings are available for purchase from the organization sponsoring the publication cited.

Single copies of NRC draft reports are available free, to the extent of supply, upon written request to the Division of Information Support Services, Distribution Section, U.S. Nuclear Regulatory Commission, Washington, DC 20555.

Copies of industry codes and standards used in a substantive manner in the NRC regulatory process are maintained at the NRC Library, 7920 Norfolk Avenue, Bethesda, Maryland, and are available there for reference use by the public. Codes and standards are usually copyrighted and may be purchased from the originating organization or, if they are American National Standards, from the American National Standards Institute, 1430 Broadway, New York, NY 10018.

NUREG/CR-5013
MEA-2232
RF, R5

Fatigue Life Characterization of Smooth and Notched Piping Steel Specimens in 288°C Air Environments

Manuscript Completed: February 1988
Date Published: May 1988

Prepared by
J. B. Terrell

Materials Engineering Associates, Inc.
Lanham, MD 20706-1837

Prepared for
Division of Engineering
Office of Nuclear Regulatory Research
U.S. Nuclear Regulatory Commission
Washington, DC 20555
NRC FIN B8900

ABSTRACT

Fatigue strain-life tests were conducted on ASME SA 106-B piping steel at 24°C (76°F) and at PWR operating temperature, 288°C (550°F), under completely reversed loading. Smooth specimens were tested at both temperatures whereas specimens containing notches of various acuities were tested at 288°C. Fatigue limits at 10^7 cycles were estimated to be 185 MPa (26.8 ksi) at 24°C and 232 MPa (33.7 ksi) at 288°C. The difference in fatigue strength observed at the PWR temperature is postulated to be due to dynamic strain aging processes. However, there is a reduction in low cycle fatigue strength at this temperature which results in a decrease in the intended safety factor of the ASME Section III design curve for carbon steels. Notch strain histories were estimated for the notched specimen tests using various interpretations of Neuber's rule. It was concluded that the use of the fatigue notch concentration factor (K_f) in the Neuber relation in conjunction with the uniaxial cyclic stress-strain curve provided the best correlation of notched specimen fatigue data with results obtained from smooth specimen tests. The notched specimen strain-life results derived from the application of Neuber's rule alone proved to be conservative when compared to smooth specimen test results to such an extent that Neuber-generated notch stress and strain amplitudes cannot be compared to the ASME Section III fatigue curves for carbon steels.

CONTENTS

LIST OF FIGURES

LIST OF FIGURES

LIST OF TABLES

FOREWORD

The work reported here was performed at Materials Engineering Associates (MEA) under the program Structural Integrity of Water Reactor Pressure Boundary Components, F. J. Loss, Program Manager. The program is sponsored by the Office of Nuclear Regulatory Research of the U. S. Nuclear Regulatory Commission (NRC). The technical monitor for the NRC is Alfred Taboada.

Prior reports under the current contract are listed below:

1. J. R. Hawthorne, "Significance of Nickel and Copper to Radiation Sensitivity and Postirradiation Heat Treatment Recovery of Reacto[illegible] Steels," USNRC Report NUREG/CR-2948, Nov. 1982.

2. "Struc[illegible] Integrity of Water Reactor Pressure Boundary Components, [illegible]al Report for 1982," F. J. Loss, Ed., USNRC Report NUREG[illegible]228, Vol. 1, Apr. 1983.

3. J. R. Hawthorne, "Exploratory Assessment of Postirradiation Heat Treatment Variables in Notch Ductility Recovery of A 533-B Steel," USNRC Report NUREG/CR-3229, Apr. 1983.

4. W. H. Cullen, K. Torronen, and M. Kemppainen, "Effects of Temperature on Fatigue Crack Growth of A 508-2 Steel in LWR Environment," USNRC Report NUREG/CR-3230, Apr. 1983.

5. "Proceedings of the International Atomic Energy Agency Specialists' Meeting on Subcritical Crack Growth," Vols. 1 and 2, W. H. Cullen, Ed., USNRC Conference Proceeding NUREG/CP-0044, May 1983.

6. W. H. Cullen, "Fatigue Crack Growth Rates of A 508-2 Steel in Pressurized, High-Temperature Water," USNRC Report NUREG/CR-3294, June 1983.

7. J. R. Hawthorne, B. H. Menke, and A. L. Hiser, "Notch Ductility and Fracture Toughness Degradation of A 302-B and A 533-B Reference Plates from PSF Simulated Surveillance and Through-Wall Irradiation Capsules," USNRC Report NUREG/CR-3295, Vol. 1, Apr. 1984.

8. J. R. Hawthorne and B. H. Menke, "Postirradiation Notch Ductility and Tensile Strength Determinations for PSF Simulated Surveillance and Through-Wall Specimen Capsules," USNRC Report NUREG/CR-3295, Vol. 2, Apr. 1984.

9. A. L. Hiser and F. J. Loss, "Alternative Procedures for J-R Curve Determination," USNRC Report NUREG/CR-3402, July 1983.

10. A. L. Hiser, F. J. Loss, and B. H. Menke, "J-R Curve Characterization of Irradiated Low Upper Shelf Welds," USNRC Report NUREG/CR-3506, Apr. 1984.

11. W. H. Cullen, R. E. Taylor, K. Torronen, and M. Kemppainen, "The Temperature Dependence of Fatigue Crack Growth Rates of A 351 CF8A Cast Stainless Steel in LWR Environment," USNRC Report NUREG/CR-3546, Apr. 1984.

12. "Structural Integrity of Light Water Reactor Pressure Boundary Components -- Four-Year Plan 1984-1988," F. J. Loss, Ed., USNRC Report NUREG/CR-3788, Sep. 1984.

13. W. H. Cullen and A. L. Hiser, "Behavior of Subcritical and Slow-Stable Crack Growth Following a Postirradiation Thermal Anneal Cycle," USNRC Report NUREG/CR-3833, Aug. 1984.

14. "Structural Integrity of Water Reactor Pressure Boundary Components: Annual Report for 1983," F. J. Loss, Ed., USNRC Report NUREG/CR-3228, Vol. 2, Sept. 1984.

15. W. H. Cullen, "Fatigue Crack Growth Rates of Low-Carbon and Stainless Piping Steels in PWR Environment," USNRC Report NUREG/CR-3945, Feb. 1985.

16. W. H. Cullen, M. Kemppainen, H. Hanninen, and K. Torronen, "The Effects of Sulfur Chemistry and Flow Rate on Fatigue Crack Growth Rates in LWR Environments," USNRC Report NUREG/CR-4121, Feb. 1985.

17. "Structural Integrity of Water Reactor Pressure Boundary Components: Annual Report for 1984," F. J. Loss, Ed., USNRC Report NUREG/CR-3228, Vol. 3, June 1985.

18. A. L. Hiser, "Correlation of C_v and K_{Ic}/K_{Jc} Transition Temperature Increases Due to Irradiation," USNRC Report NUREG/CR-4395, Nov. 1985.

19. W. H. Cullen, G. Gabetta, and H. Hanninen, "A Review of the Models and Mechanisms For Environmentally-Assisted Crack Growth of Pressure Vessel and Piping Steels in PWR Environments," USNRC Report NUREG/CR-4422, Dec. 1985.

20. "Proceedings of the Second International Atomic Energy Agency Specialists' Meeting on Subcritical Crack Growth," W. H. Cullen, Ed., USNRC Conference Proceeding NUREG/CP-0067, Vols. 1 and 2, Apr. 1986.

21. J. R. Hawthorne, "Exploratory Studies of Element Interactions and Composition Dependencies in Radiation Sensitivity Development," USNRC Report NUREG/CR-4437, Nov. 1985.

22. R. B. Stonesifer and E. F. Rybicki, "Development of Models for Warm Prestressing," USNRC Report NUREG/CR-4491, Jan. 1987.

23. E. F. Rybicki and R. B. Stonesifer, "Computational Model for Residual Stresses in a Clad Plate and Clad Fracture Specimens," USNRC Report NUREG/CR-4635, Oct. 1986.

24. D. E. McCabe, "Plan for Experimental Characterization of Vessel Steel After Irradiation," USNRC Report NUREG/CR-4636, Oct. 1986.

25. E. F. Rybicki, J. R. Shadley, and A. S. Sandhu, "Experimental Evaluation of Residual Stresses in a Weld Clad Plate and Clad Test Specimens," USNRC Report NUREG/CR-4646, Oct. 1986.

26. "Structural Integrity of Water Reactor Pressure Boundary Components: Annual Report for 1985," F. J. Loss, Ed., USNRC Report NUREG/CR-3228, Vol. 4, June 1986.

27. G. Gabetta and W. H. Cullen, "Application of a Two-Mechanism Model for Environmentally-Assisted Crack Growth," USNRC Report NUREG/CR-4723, Oct. 1986.

28. W. H. Cullen, "Fatigue Crack Growth Rates in Pressure Vessel and Piping Steels in LWR Environments," USNRC Report NUREG/CR-4724, Mar. 1987.

29. W. H. Cullen, M. E. Mayfield, and M. R. Jolles, "Fatigue Crack Growth of Part-Through Cracks in Pressure Vessel and Piping Steels: Air Environment Results, USNRC Report NUREG/CR-4828 (in publication).

30. D. E. McCabe, "Evaluation of Surface Cracks Embedded in Reactor Vessel Cladding Unirradiated Bend Specimens," USNRC Report NUREG/CR-4841, May 1987.

31. H. Hanninen, M. Vulli, and W. H. Cullen, "Surface Spectroscopy of Pressure Vessel Steel Fatigue Fracture Surface Films Formed in PWR Environments," USNRC Report NUREG/CR-4863, July 1987.

32. A. L. Hiser and G. M. Callahan, "A User's Guide to the NRC's Piping Fracture Mechanics Data Base (PIFRAC)," USNRC Report NUREG/CR-4894, May 1987.

33. "Proceedings of the Second CSNI Workshop on Ductile Fracture Test Methods (Paris, France, April 17-19, 1985)," F. J. Loss, Ed., USNRC Conference Proceeding NUREG/CP-0064, (in publication).

34. W. H. Cullen and D. Broek, "The Effects of Variable Amplitude Loading on A 533-B Steel in High-Temperature Air and Reactor Water Environments," USNRC Report NUREG/CR-4929 (in publication).

35. "Structural Integrity of Water Reactor Pressure Boundary Components: Annual Report for 1986," F. J. Loss, Ed., USNRC Report NUREG/CR-3228, Vol. 5, July 1987.

36. F. Ebrahimi et. al, "Development of a Mechanistic Understanding of Radiation Embrittlement in Reactor Pressure Vessel Steels: Final Report," USNRC Report NUREG/CR-5063, Jan. 1988.

ACKNOWLEDGMENTS

The author wishes to express his appreciation to the following people who helped make this work possible: Greg Baker for his experience with test systems and for his conscientious effort in conducting the tests, Bob Taylor for his helpful suggestions, Gray Carlson, Sandra Wassam, Leah Cargill, June Phillips, and Jodi Sprecher for their valuable efforts in assembling the manuscript, the students who have assisted in testing, Prof. Norm Dowling for his consulting expertise, Dr. William H. Cullen for his sharing of experience of fatigue testing and his enthusiastic support, and Dr. Frank J. Loss whose overall direction for this research has been instrumental to the entire effort.

Special thanks is extended to Milt Vagins, Al Taboada, and Mike Mayfield of the Nuclear Regulatory Commission for their enthusiatic support and direction of this effort.

1. INTRODUCTION

Fatigue life estimation of structural components having geometric discontinuities has long been an area that has generated considerable attention. Stress raisers such as those present at joints, angles, weldments, holes, thread roots, etc. are almost always the site for the nucleation and growth of fatigue cracks in structural elements subjected to fatigue loading. A key element in predicting the fatigue life of a notched member is an accurate assessment of the strain history at the notch root. There have been a number of analytical estimation schemes which have attempted to model cyclic notch strains (Refs. 1 - 3) of which Neuber's rule (Ref. 3) appears to be favored by most investigators who study fatigue crack nucleation and total fatigue life. Neuber's rule enjoys an advantage over other notch analysis methods when both accuracy and simplicity of use are considered. However, a survey of the literature quickly reveals that a number of Neuber's rule variations have been employed for the purpose of estimating notch root strain histories. Some of these variations are described in the text below.

The primary purposes of this investigation are (1) to characterize the strain-life behavior of SA 106-B piping steel at room temperature and at temperatures typical of pressurized water reactor (PWR) environments, (2) to determine the appropriate form of Neuber's rule which most accurately correlates notched specimen fatigue life behavior with that of smooth specimens, and (3) to determine whether or not Neuber-generated notch strains (and hence, pseudostresses) can be accurately correlated with the ASME Boiler and Pressure Vessel Code Section III stress-life (S-N) design curves for carbon steels. These results will be used in the next step of this investigation in which the strain-life behavior of SA 106-B steel in the presence of simulated PWR environments having low dissolved oxygen will be assessed. The end result will lead to the development of a data base that could be used to formulate revisions to the ASME Section III curves.

2. BACKGROUND

The most accepted method by which to analytically estimate stresses and strains at the root of a notch is with the use of Neuber's rule (Ref. 3). Neuber based his rule on the assumption that there must exist a function which consists of a geometric mean value of stress, deformation, and concentration factor which has the same value for any stress-strain law. The rule was derived for a notch having a zero degree angle but can be applied to all notches since it was found that the influence of notch angle on the notch root stress and strain values was insignificant (Ref. 3). Neuber stated that the geometric mean value of stress and strain concentration factors (K_σ and K_ε, respectively) with any stress-strain law is equal to the theoretical stress concentration factor and is noted as:

$$K_t = (K_\varepsilon K_\sigma)^{1/2} \tag{1}$$

Application of Neuber's rule has been successful even when applied loads have approached general yielding. When compared to more rigorous analyses such as finite element methods (Ref. 4), Neuber's rule yields higher notch root stress and strain values and therefore inherently tends to be more conservative. Figure 1 shows a plot of stress and strain concentration factors from both finite element analysis and Neuber's rule as a function of normalized stress for both plane stress and plane strain conditions. The geometric mean of K_ε and K_σ from Neuber is larger (and therefore, more conservative) than K_ε and K_σ from the finite element analysis.

Neuber's rule was first used to provide indices of equal fatigue damage for notched and unnotched specimens by describing the inelastic behavior during fatigue life prediction of notched aluminum specimens (Ref. 5). Figure 2 shows excellent agreement in the comparison between notched specimen fatigue data and smooth specimen data for 7075-T6 aluminum using the fatigue notch factor (K_f) in the Neuber relation. The solid data points represent tests performed when gross yielding of the entire specimen occurred. The open data points represent specimens tested when the gross cross-section remained elastic. These tests were performed with completely-reversed loading which resulted in zero mean stress. Non-zero mean stress resulted in errors in predicted life and was avoided. However, even during the normal course of completely-reversed fatigue cycling, large tensile loads tended to induce compressive residual stresses, but this effect was somewhat counteracted by the process of residual stress relaxation at notch roots because sufficient plastic strain was present (Refs. 6, 7).

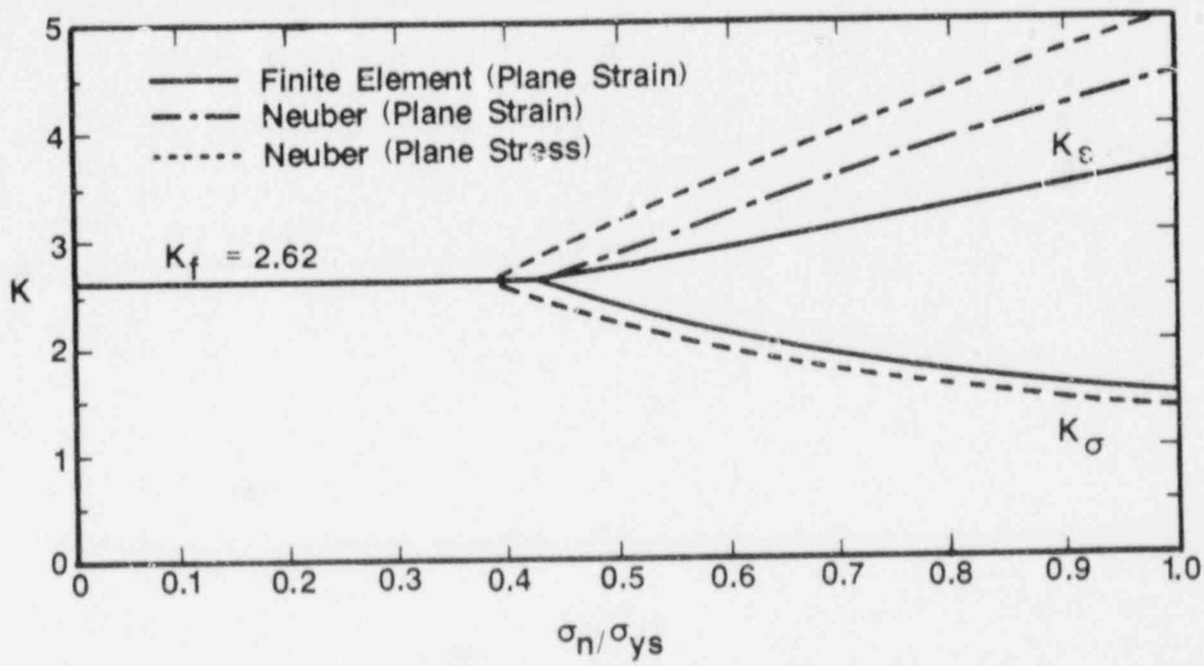

Fig. 1 Stress and strain concentration factors from both Neuber's rule and finite-element analysis as a function of normalized stress for both plane stress and plane strain conditions (Ref. 4). K is defined as a generalized notch concentration factor and σ_n and σ_{ys} are the nominal and yield stresses, respectively.

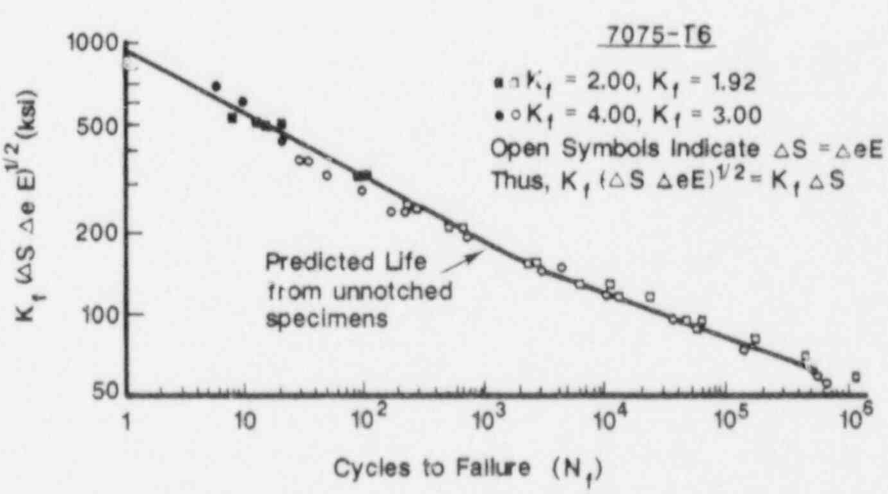

Fig. 2 Fatigue life curve of notched 7075-T6 aluminum specimens correlated, using Neuber's rule, to smooth specimen fatigue results (Ref. 5). 1 ksi = 6.895 MPa.

Neuber's rule (Eq. 1) can be more conveniently used by substituting the following expressions for K_σ:

$$K_\sigma = \frac{\sigma}{S} = \frac{\text{stress at the notch root}}{\text{unnotched stress}} \quad (2)$$

$$K_\varepsilon = \frac{\varepsilon}{e} = \frac{\text{strain at the notch root}}{\text{unnotched strain}} \quad (3)$$

Rearranging and multiplying by E (elastic modulus) yields:

$$K_t \ (S_a e_a E)^{1/2} = (\sigma_a \varepsilon_a E)^{1/2} \quad (4)$$

which is valid for both plastic and elastic gross and local stresses and strains. Stresses and strains in Eq. 4 have been written in terms of amplitudes which have been designated with the subscript "a". This convention will be carried throughout the remainder of this report. When gross stresses and strains are elastic but local (notch root) stresses and strains are plastic, $S_a = Ee_a$ can be substituted in the left-hand side of Eq. 4:

$$K_t S_a = (\sigma_a \varepsilon_a E)^{1/2} \quad (5)$$

For situations where local stresses and strains are elastic, Eq. 5 reduces to the familiar expression for the elastic theoretical notch factor:

$$K_t S_a = \sigma_a \quad (6)$$

The most important feature of the Neuber relation which makes it so useful in determining notch stresses and strains is that the product of notch stress and notch strain equals a constant value for a given condition:

$$\sigma_a \varepsilon_a = \text{constant} \quad (7)$$

Of course, the quantities of σ and ε are both unknowns; therefore, another equation containing these two values must be solved simultaneously with the Neuber equation. This other equation usually describes the stress-strain behavior of the material under transient stress-strain conditions. The intersection of the Neuber equation with the cyclic stress-strain equation after material stabilization has occurred will yield the notch stress and strain values.

Figure 3 shows a series of hyperbolae, each having different values for $\varepsilon_a \sigma_a$ intersecting the cyclic stress-strain curve obtained from smooth specimens of the same metal tested at the same temperature as the notched specimens (Ref. 8). The curve is usually constructed by connecting the tips of stable hysteresis loops from constant amplitude, strain-controlled tests at different strain ranges. Procedures for determining the cyclic stress-strain behavior of a material may vary slightly (Ref. 9). The curve is usually constructed from the data obtained from an incremental step test. Figure 4 shows a strain-time trace for two blocks of strain cycles obtained by incrementally decreasing and then increasing the strain range after each cycle, and a set of hysteresis loops that correspond to one set of increments. The actual data used for construction of the cyclic stress-strain curve is usually obtained from a set of increments taken during the midlife of a specimen after stabilization of the hysteresis loop has occurred; that is, the shape and dimensions of the curve essentially remain unchanged after a prerequisite amount of cycling. Figure 5 shows the stabilization of strain with number of cycles for different strain amplitudes for tests performed in strain control under constant amplitude conditions (Ref. 10).

The equation for cyclic stress-strain is composed of elastic and plastic components of strain:

$$\varepsilon_a = \varepsilon_{ea} + \varepsilon_{pa} \tag{8}$$

where ε_a is the total strain amplitude and ε_{ea} and ε_{pa} are the elastic and plastic components of strain amplitude, respectively. Equation 8 can be rewritten as:

$$\varepsilon_a = \frac{\sigma_a}{E} + \left(\frac{\sigma_a}{A}\right)^{1/n} \tag{9}$$

where ε_a and σ_a are strain and stress amplitudes respectively, A is the cyclic strength coefficient and n is the cyclic strain hardening exponent and is the cyclic counterpart to the monotonic Ramberg-Osgood strain hardening exponent.

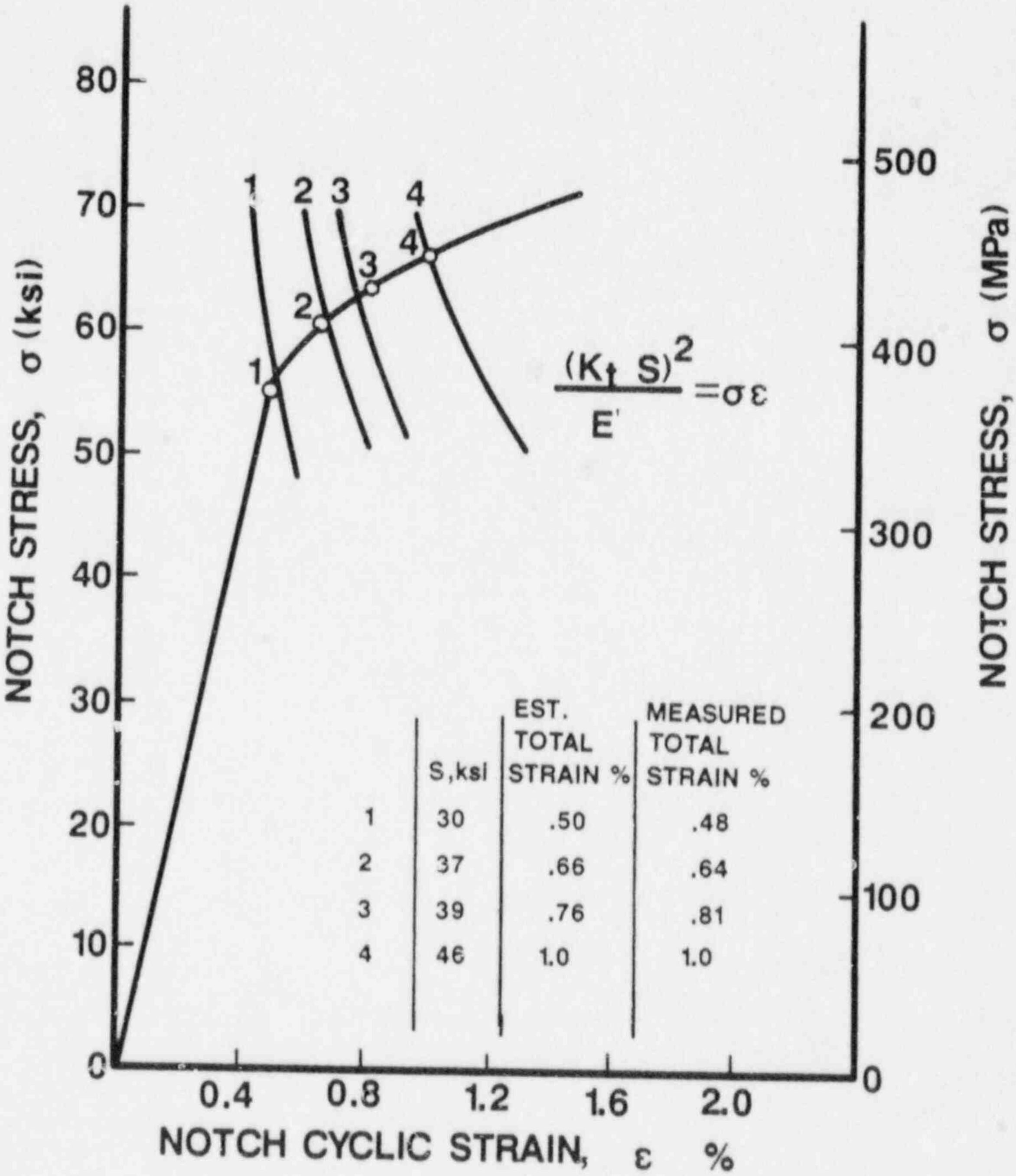

	S,ksi	EST. TOTAL STRAIN %	MEASURED TOTAL STRAIN %
1	30	.50	.48
2	37	.66	.64
3	39	.76	.81
4	46	1.0	1.0

Fig. 3 A series of $\sigma\varepsilon = (K_t S)^2/E'$ hyperbolae shown intersecting a cyclic stress-strain curve for different values of S. The intersection of each set of curves yields the notch root cyclic stress and strain values (Ref. 8).

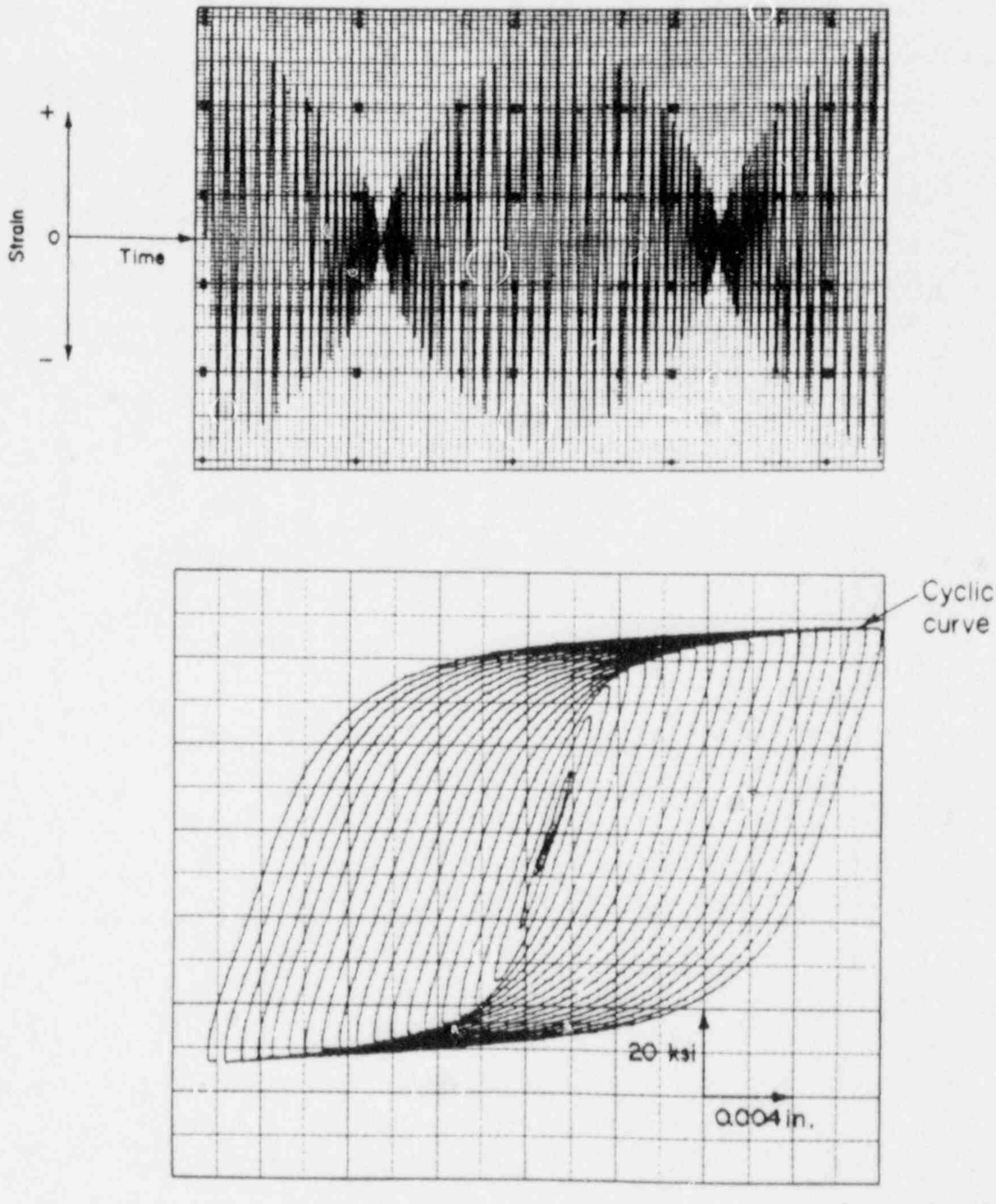

Fig. 4 Information used in the construction of a cyclic stress-strain curve. The upper figure shows two blocks of strain-time traces obtained by incrementally decreasing and then increasing the strain range for each cycle. The lower figure shows a set of hysteresis loops that correspond to one set of strain-time increments (Ref. 9).

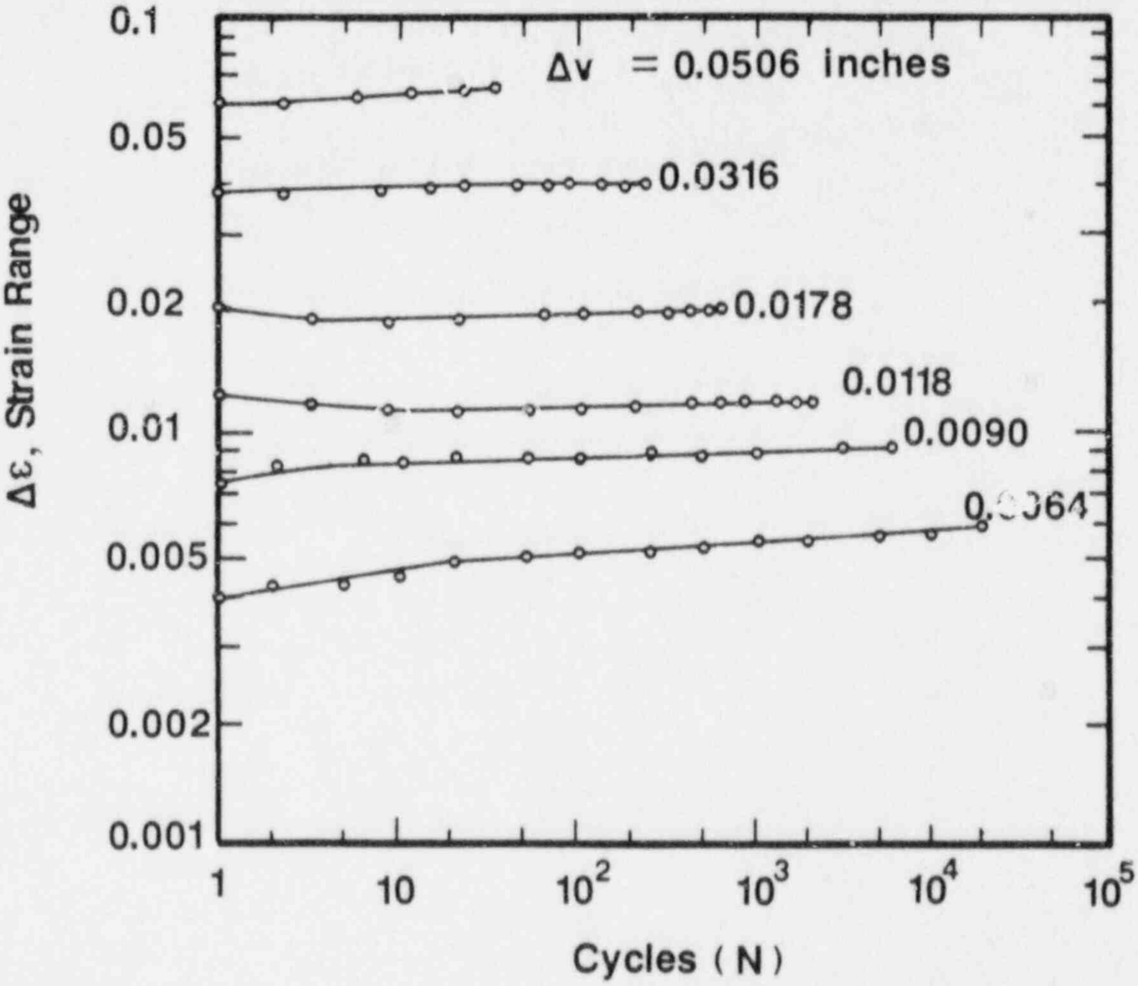

Fig. 5 Stabilization of strain range as a function of number of cycles for different deflection ranges for SA 533-B steel under constant amplitude deflection control (Ref. 10).

Equation 9 properly describes the cyclic stress-strain behavior for plane stress conditions because the material can freely undergo transverse contractions when the material is loaded. Ignoring goodness-of-fit considerations, the data used to determine the coefficient and exponent for Eq. 9 are usually obtained from small, smooth uniaxial specimens subjected to completely-reversed loading.

However, if there exists a situation in which transverse contraction in the specimen is prevented, then plane strain conditions can prevail. Of particular interest is the situation in which a notched member exhibits a thickness that is large in comparison to the notch root radius. As a result, the material at the notch root cannot contract and a biaxial stress state is assumed to exist. Consequently, the notch root material will not obey a stress-strain law such as the one presented in Eq. 9. Modification of the stress-strain law for plane strain conditions must be made for the first principal stress direction (Ref. 11). These modifications yield the following equation for plane strain cyclic stress-strain estimation:

$$\varepsilon'_{1a} = \frac{\sigma'_{1a}}{E'_1} + \left(\frac{\sigma'_{1a}}{A'}\right)^{1/n'} \qquad (10)$$

where

E'_1, the modified elastic modulus is

$$E'_1 = \frac{E}{1 - \nu^2} \qquad (11)$$

ν, the generalized Poisson's ratio applicable to total strain is

$$\nu = \frac{\nu_e + \dfrac{E\varepsilon_{pa}}{2\sigma_a}}{1 + \dfrac{E\varepsilon_{pa}}{\sigma_a}} \qquad (12)$$

σ'_{1a}, the stress amplitude in the first principal direction is

$$\sigma'_{1a} = \frac{\sigma_a}{1 - \nu + \nu^2} \qquad (13)$$

ε'_{1a}, the strain amplitude in the first principal direction is

$$\varepsilon'_{1a} = \frac{\varepsilon_a(1 - \nu^2)}{\sqrt{1 - \nu + \nu^2}} \qquad (14)$$

where

ν_e is Poisson's ratio for the elastic case, A' is the cyclic strength coefficient, and n' is the cyclic strain hardening exponent. A' and n' are fitted to the cyclic stress-strain equation modified for plane strain.

In order to experimentally determine the local stresses and strains using Neuber's rule, the investigator needs only a few pieces of engineering information. First, the loading history must be known. Second, knowledge of the notch geometry, and hence, K_t is needed. Many sources are available to help in the determination of K_t. One of the best sources is the handbook on stress concentration factors by Peterson (Ref. 12). K_t is presented for most simple specimen geometries as a function of geometry and loading mode in graphical form. K_t for more complex geometries, such as that for compact tension specimens, can be determined through finite element analysis programs (Refs. 13 - 16) or equivalent advanced analytical techniques. Third, the smooth specimen cyclic stress-strain curve is obtained using completely-reversed loading under identical conditions as the ensuing testing is needed. Analytical analysis can be greatly facilitated if Eq. 9 is fitted to the curve.

As previously mentioned, the application of Neuber's rule in the determination of notch stresses and strains during fatigue loading involves the use of a notch concentration factor in the calculation. Examination of the literature shows that a number of variations on Neuber's original rule have been employed. Dowling et al. (Ref. 11) and Leax et al. (Ref. 17) used the theoretical elastic stress concentration factor K_t in their assessment of fatigue life predictions for specimens tested with various notch acuities, temperatures, and mean stresses. Plane strain conditions were assumed to prevail in the notched compact tension specimens used in Reference 11, so the plane strain version of the cyclic stress strain equation was used in conjunction with the Neuber relation involving K_t. Center-notched plate specimens were used by Leax, et al. (Ref. 17) in which plane stres conditions prevailed; therefore, the plane stress cyclic stress-strain equation was used. More pursuantly, the notched specimen stress-life data were collapsed onto curves obtained by testing smooth specimens. Most of the data were accumulated for lives greater than 10^3 cycles when the elastic strain amplitude components of the total strain were considerably larger than the corresponding plastic strain components.

Other investigators have used K_t in studies that combined crack initiation with crack propagation in their assessment of total life (Refs. 18 - 20). Specimens such as notched compact tension specimens and center-cracked specimens have been proven useful for combined crack initiation and propagation studies. Usually the crack initation event was detected optically. Fracture mechanics relations modeled the crack growth rate to the point beyond which the crack length reached a size which was considered failure. Finally, the initiation and propagation components of specimen life were summed for all specimens and plotted against local stress amplitude. Figure 6 shows the analytical and experimental results of Socie, et al. (Ref. 19) for blunt and sharpened notched specimens of AISI 4030 steel. Their results show that the crack initiation event occurs very early in the life of sharply notched specimens in contrast to crack initation behavior in bluntly-notched members.

While conducting fatigue studies in high pressure, high temperature water environments, Prater and Coffin (Refs. 21, 22) "married" the concepts of Neuber with fracture mechanics expressions as a function of notch geometry, with the result being an expression for notch root strain amplitude as a function of cyclic stress intensity and notch root radius. The expression

$$\Delta\sigma = \Delta K \; (\pi\rho)^{-0.5} \qquad (15)$$

where ρ is the notch root radius, and ΔK is the range in stress intensity, was used to relate the stress amplitude with the stress intensity and notch root radius for compact tension specimens. After combining Eq. 15 with Neuber's rule, they obtained the expression

$$\varepsilon_a \; E = \Delta K_I^2 \; (\pi e \sigma_a)^{-1} \qquad (16)$$

which assumed that ρ was sufficiently small so as to introduce insignificant error in the fracture mechanics relation (Eq. 15).

The notched compact tension specimens used in the Prater and Coffin studies were 25.4-mm (1-in.) thick and presumably exhibited plane strain conditions at the root of the notch. A cyclic stress-strain relation was not used in their analysis; instead, a relation for nominal stress for compact tension specimens was used:

$$\Delta S = \Delta P \quad \frac{3(W + a)}{(W - a)^2} + \frac{1}{W - a} \qquad (17)$$

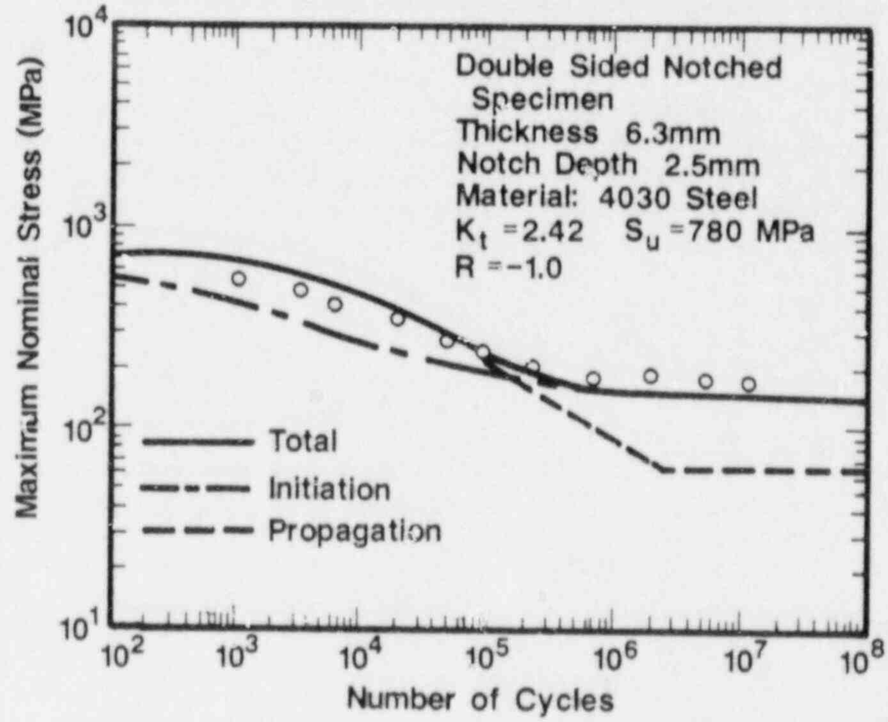

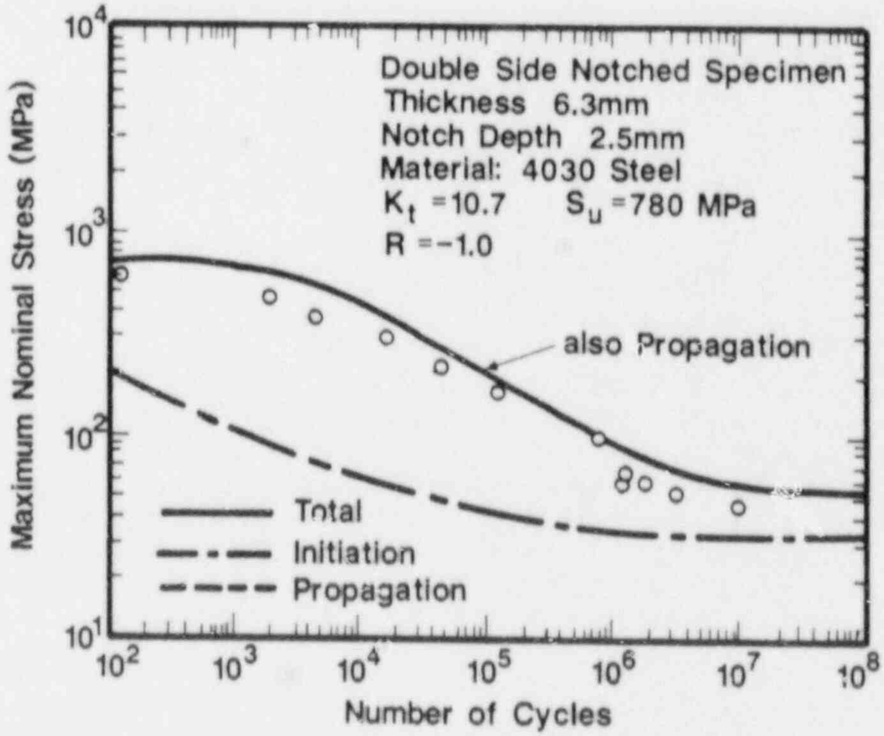

Fig. 6 Fatigue life estimations determined by summing crack initiation and propagation lives for alloy steel specimens having two notch acuities (Ref. 19).

where ΔS and ΔP are the stress and load range, respectively, and W and a are the total and notch depth of the specimen, respectively, measured from the load line. However, their method of testing and analysis yielded strain amplitude values that were much too high, and they attributed this to the anomalies encountered when dealing with sharply notched fatigue data. In an attempt to remedy this problem, the concept of "worst-case notch" (Refs. 23, 24) was incorporated into their analysis to help interpret their data. This concept attempts to explain why no further influence of notch stress concentration factor is observed in fatigue life results as the notch root radius is decreased below a specific, empirically-determined dimension. For their test specimen geometry, the value of worst-case notch root radius was determined to be 0.165 mm (0.0065 in.). Their data were fitted to the ASME mean fatigue data line for carbon steels (Ref. 25). While this concept did allow a fit of the data and is believed to be viable since the number of cycles needed to initiate a fatigue crack is believed to be related to the size of the plastically deformed material in the vicinity of the notch base, it is, when fitted to the ASME Sec. III design curve, a factor which does not allow for assessment of local strains at the notch base.

The use of K_f in notched specimen fatigue work has been carried out by a number of investigators (Ref. 5 - 7 and 26 - 29). Wetzel (Ref. 7) accurately predicted local strain histories using Neuber's rule for thin, notched aluminum plates that were also subjected to strain measurements from zero to maximum loading. The resulting local stresses were used to estimate the life of a notched member by relating the Neuber-generated local stress measurements to stress-life plots obtained from smooth specimens (see Fig. 7). Topper, et al. (Ref. 5) used Neuber's rule to convert smooth specimen data for thin, notched aluminum plates into a stress-life plot which could be used to estimate the fatigue life of any notched member made from that particular metal. Figure 2 contains a plot of their results. Topper, et al. (Ref. 6) extended the use of Neuber's rule to cumulative damage studies to determine the influence of loading sequence, number of loading blocks, and mean stress influence on fatigue damage summations based on cyclic strains. It was found that the principles used in studying cumulative damage using smooth specimens under strain control are applicable to the notched specimen fatigue problem via the use of Neuber's rule. The accepted rationale for preference of K_f over K_t in the aforementioned studies was based on the observation that as the notch becomes sharper, K_t always overestimates the notch effect during fatigue.

Socie (Ref. 26) used Neuber's rule with K_f as a means to determine notch stresses and strains in a computer-aided analysis of variable amplitude fatigue loading spectra. Baus, et al. (Ref. 27) found an excellent correlation between fatigue crack initiation and the low cycle fatigue behavior of 15-mm (0.6-in.) thick compact tension specimens made from high strength steel when the number of cycles to initiation was below 10^5 cycles. They contended that the propagation phase of fatigue life was very short in comparison to the initiation life, and that both $\Delta\sigma\Delta\varepsilon$ and $\Delta\varepsilon$ remain essentially constant at the notch root because of rapid stabilization of the notch root

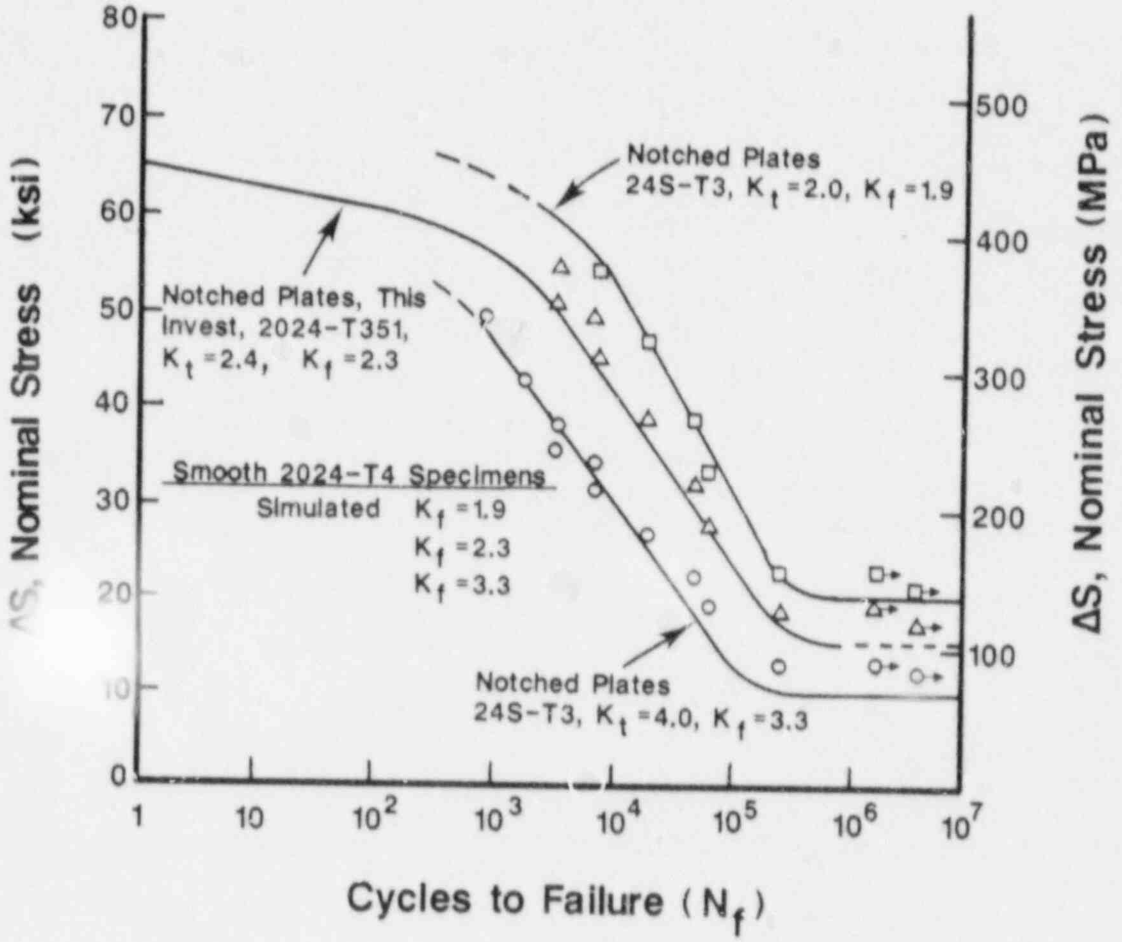

Fig. 7 Estimation of fatigue life for notched aluminum plates by relating Neuber-generated local stress measurements to fatigue life plots obtained from smooth specimens (Ref. 7).

material. Maiya (Ref. 28) found that the use of K_f led to more accurate estimates of fatigue crack initiation whereas the use of K_t significantly underpredicted the experimental initiation life with the deviation becoming more severe at higher values of K_t. The plane strain state of stress was approached in their circumferentially notched round bars made from Type 304 stainless steel specimens tested under completely-reversed axial loading at 593°C (1100°F). Saanouni and Bathias (Ref. 29) studied crack initiation life using both notched compact tension and round bar specimens using K_f and a modified expression for the characteristic length (ρ') in the Neuber expression that relates K_f to K_t:

$$K_f = 1 + \frac{K_t - 1}{1 + \sqrt{\frac{\rho'}{r}}} \tag{18}$$

The significance of ρ' is that it represents a distance from the notch tip beyond which there exists no more stress gradient. Their characteristic length modification accounted for the plastic deformation concentrated at the notch tip and allowed for a better fit of their data.

Some investigators have contended that a modification which accounts for inelastic net section behavior must be applied to Neuber's rule. Seeger and Heuler (Ref. 30) performed a fatigue analysis using such a modified version in the following modified form:

$$\sigma_a \, \varepsilon_a = \frac{K_t^2 \, S_a S_p e_a^*}{\sigma_y} \tag{19}$$

S_p represents the nominal stress amplitude required to produce net section yielding and e^*_a is a nominal modified strain amplitude value. S_p can be regarded as the stress at fully plastic limit load and usually has a higher value than the nominal stress through the notched area due to transverse stresses that arise from constraint. S_p is usually approximated from finite element analysis or from application of Henkey's flow rules assuming an elastic-perfectly plastic material law. The value e_a* is obtained from the cyclic stress-strain curve by entering the value

$$S_a^* = S_a \frac{\sigma_y}{S_p} \tag{20}$$

This method, applied to center hole and compact tension specimens, approximates actual load-strain behavior measured with strain gages. Socie, et al. (Ref. 19) applied Seeger and Heuler's method to estimation of fatigue lives for double-edged notched, notched compact tension, and center notched specimens made from medium and high strength steels having various blunt notch acuities. Their experimental data agreed fairly well with their analytical estimates.

Questions concerning the value of the proper notch factor constant for use in Neuber's rule have previously arisen and been addressed (Refs. 28, 31). Leis, et al. (Ref. 31) performed a deformation analysis in which Neuber's rule was rewritten in terms of K_t, smooth specimen stresses and strains, and nominal (net section) stresses and strains for notched members and was compared with the Neuber expression relating K_f to the same parameters for stress and strain. Experimental measurements of notch stresses and strains were obtained with strain gages mounted onto notched plates of high strength aluminum and low strength mild steel and were compared to the deformation analysis. It was found that fatigue predictions were valid for notched specimens based on the assumption that equal lives to crack initiation were obtained in both smooth and notched specimens having identical strain histories at the notch root (see Fig. 8), thereby indicating that any discrepancies between K_t and K_f may not be attributed to size effects, but must be attributed to changes in the ratio of nominal to notch deformations. It was also shown by Leis, et al. (Ref. 31) and by Maiya (Ref. 28) that the K_t factor was a valid parameter for elastic transient deformation, but was not valid for plastic deformations, and that an experimentally determined K_f accurately predicts stable notch root deformation (see Figs. 9, 10). Walker (Ref. 8) further investigated the use of K_t and K_f and found that the stress state in the vicinity of the notch must be taken into consideration. Double edge notched plates of high strength aluminum were strain gaged; the measured strains were compared to strains obtained from analytical modeling of plasticity effects. It was concluded that the use of K_f in Neuber's rule with a uniaxial stress-strain law yields the same results as the use of K_t in Neuber's rule with a multiaxial stress strain law when the notch behaves elastically (Fig. 11). Examination of sharp notch fatigue data suggests that the use of K_t with a multiaxial stress-strain law would lead to more accurate strain approximations because the plastic strain is not overestimated (Fig. 12).

In summary, nearly 30 years of the development of Neuber's rule has led to several successful applications in the analysis of notched specimens of various geometries and material types. Methods of introducing K_t and K_f into expressions based on Neuber's rule have been applied to strain-life, stress-life, crack initiation, and total life estimations of structural elements. In short, the use of K_t has historically yielded accurate results when applied to stress-life notched specimen fatigue analyses and in total life predictions based on summation of crack initiation and crack propagation lives. The use of K_f has generally yielded accurate results when strain-life curves for notched elements were estimated.

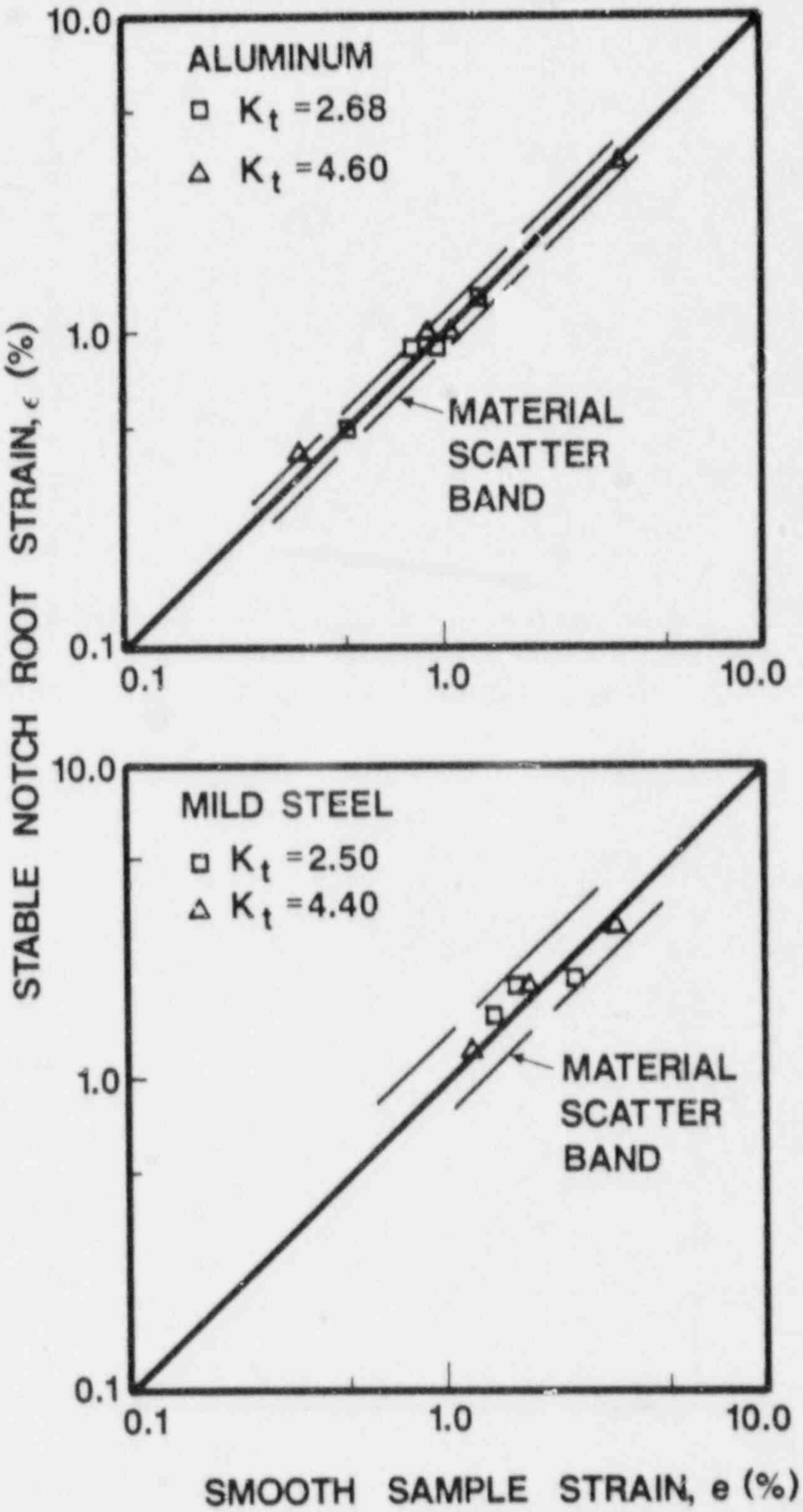

Fig. 8 Comparison of smooth sample strains with stable notch root strains at equal crack initiation lives. Notch root strains were estimated with Neuber's rule (Ref. 31).

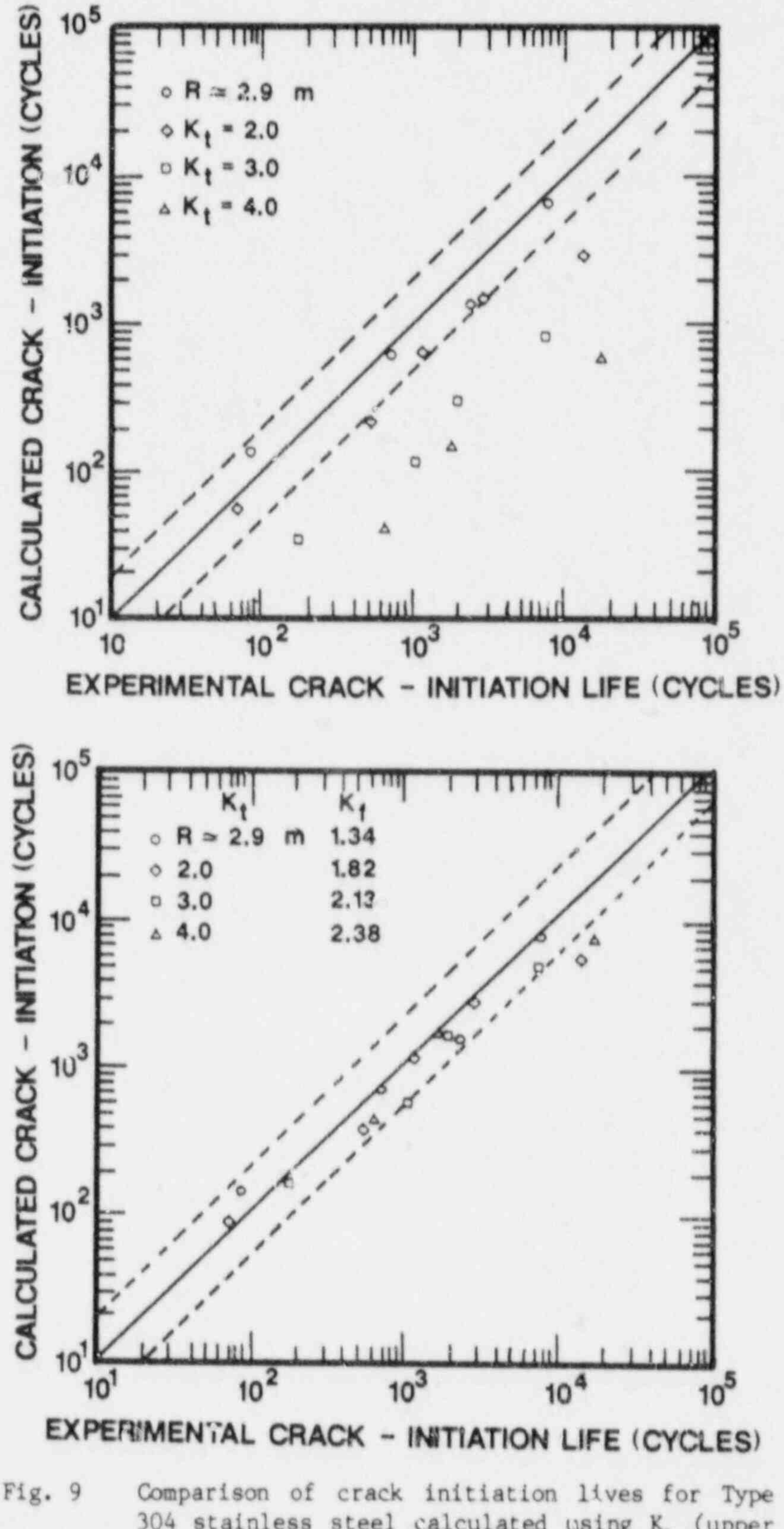

Fig. 9 Comparison of crack initiation lives for Type 304 stainless steel calculated using K_t (upper plot) and K_f (lower plot). For sharper notches, K_f more accurately predicts crack initiation lives (Ref. 28).

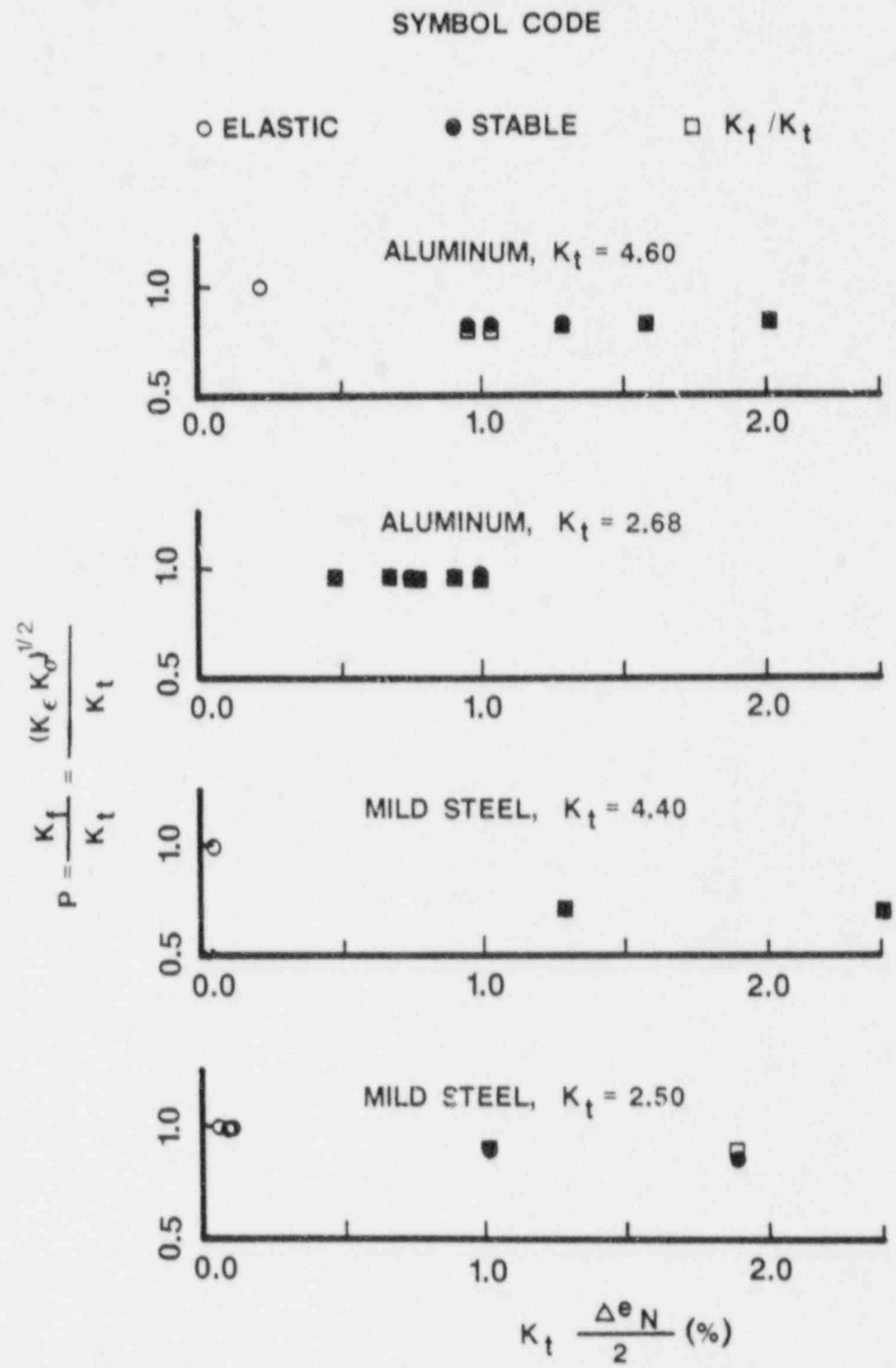

Fig. 10 K_f/K_t vs. $K_t e_{a, nominal}$ showing inability of K_t to characterize inelastic notch root strains (Ref. 31).

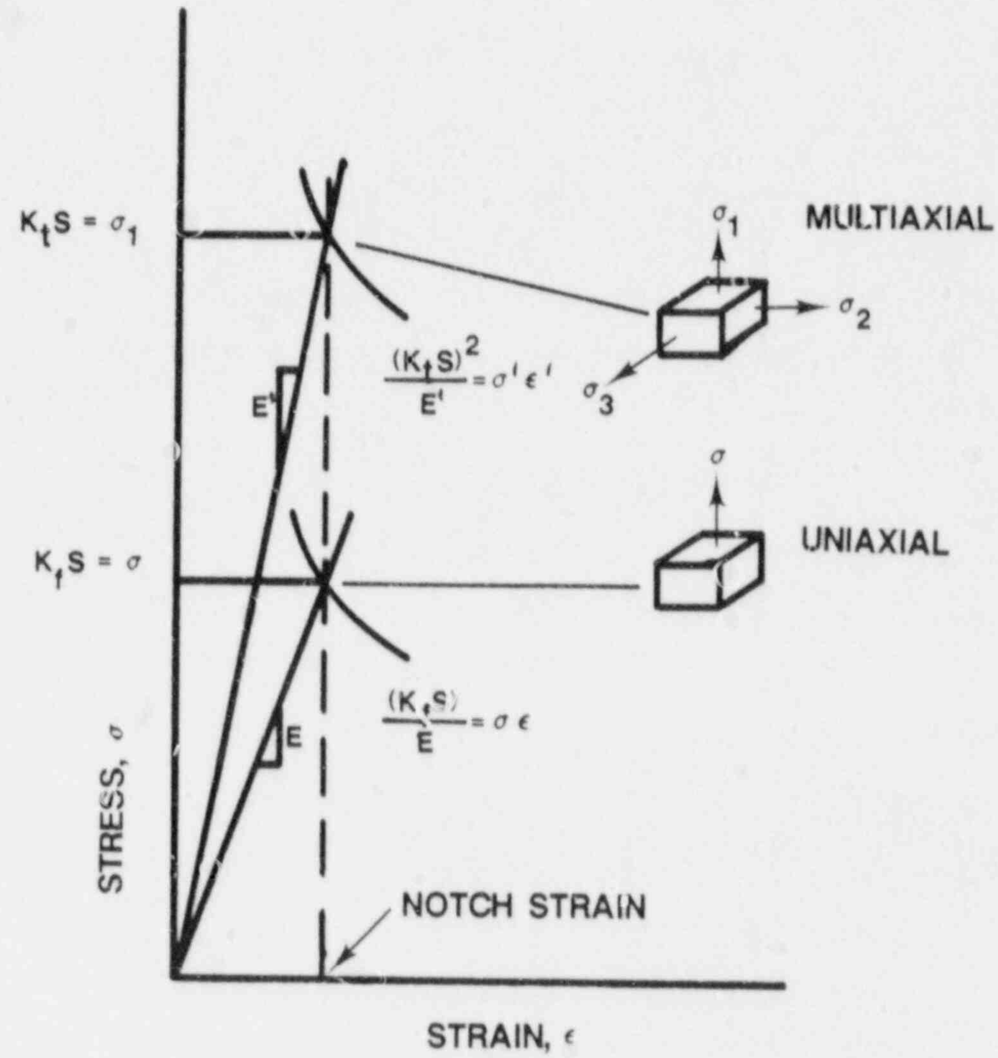

Fig. 11 Elastic notch stresses calculated using either K_t or K_f in Neuber's rule with a multiaxial stress-strain law vs. notch strain, showing that either type of elastic notch stress calculation should result in the same value for elastic notch strain (Ref. 8).

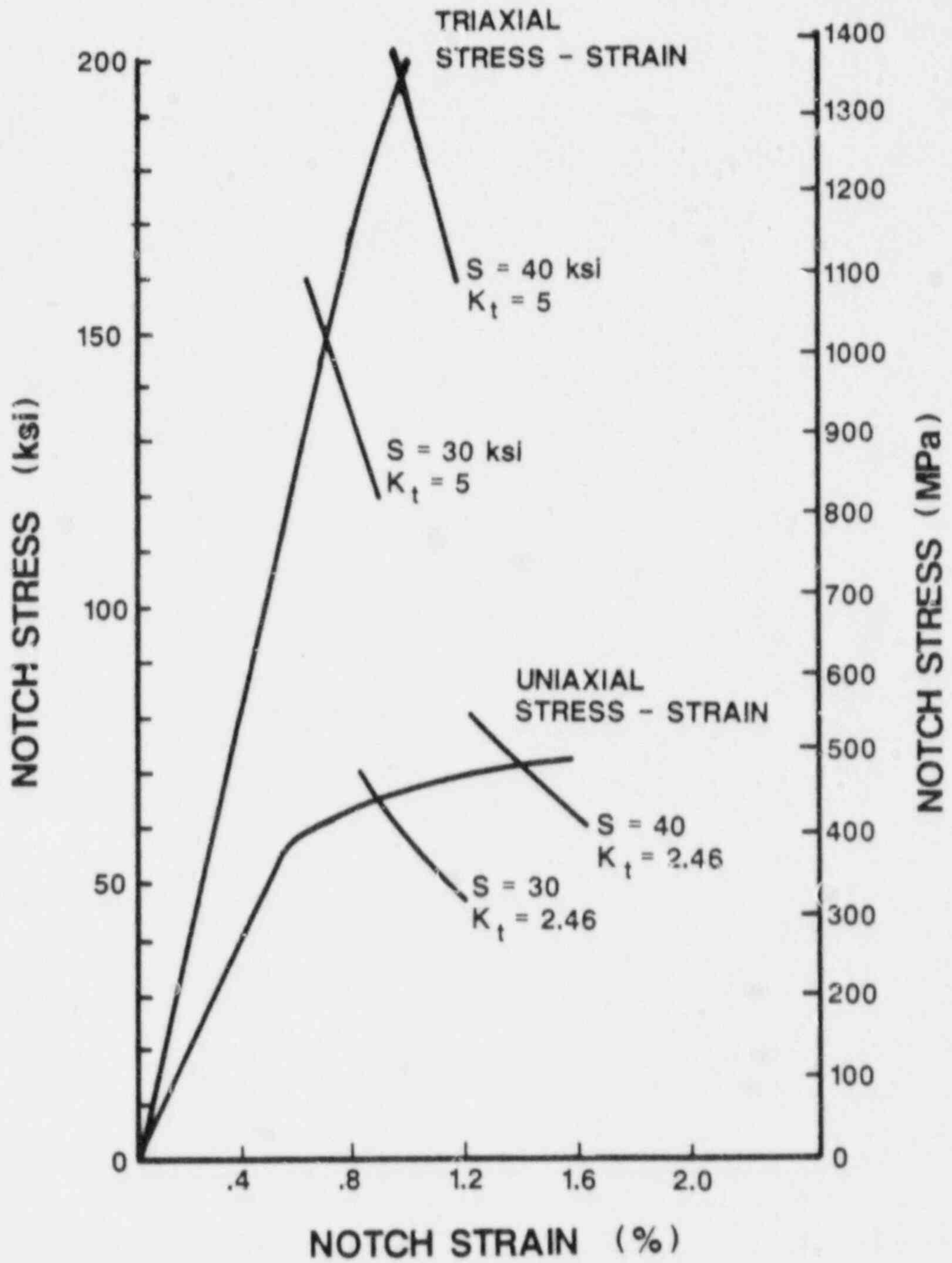

Fig. 12 Notch stresses vs. notch strains for a sharp notch estimated by using K_t in Neuber's Rule with either a triaxial or uniaxial stress-strain law. The former estimation, according to Ref. 31, should result in more accurate estimations of notch root stresses and strains (Ref. 8).

In the study of described below, strain-life tests of smooth and circumferentially notched, round bar specimens as SA 106-B piping steel have been completed, and notch strain analysis results were correlated with data acquired from smooth specimen results as a measure of the degree of accuracy of the Neuber's rule analysis methods.

3. EXPERIMENTAL PROCEDURE

The material used in this investigation is SA 106-B 203-mm (8-in.) Schedule 100 steel pipe. Its chemical composition is given in Table 1 and the room temperature tensile properties are given in Table 2. Microstructural samples were prepared and are shown in Figs. 13 and 14. The microstructure consists of elongated grains of free ferrite and grains consisting of finely-spaced lamellar pearlite. Microhardness surveys yielded an average value of 169 KHN for the free ferrite and 262 KHN for the pearlite. ASTM grain size was from 7 to 8 and the inclusion count was 1.5 for silicates. Figure 14 shows the distribution of the silicate inclusions.

Table 1 Chemical Composition (in wt. %) of SA 106-B Steel Used in this Investigation

C	S	Si	Mo	Cr	Ni	Mn	P	N
0.26	0.020	0.28	0.003	0.015	0.002	0.92	0.008	0.0069

Table 2 Average Mechanical Properties of SA 106-B Steel Test Temperature: 24°C (76°F)

Yield Strength		Ultimate Strength		Elongation	Reduction in Area
(MPa)	(ksi)	(MPa)	(ksi)	(%)	(%)
300	43.5	522.6	75.8	36.6	66.3

Specimen blanks were sawed from the pipe wall as shown in Fig. 15. Smooth specimens were machined in compliance with ASTM E 606-85 (Ref. 32) according to Fig. 16. All of the notched specimens were machined according to Fig. 17. The nominal (net section) diameter (d) for all notched specimens was 6.35 mm (0.250 in.), which was the same as for the smooth specimens. The major (or gross) diameter (D) and the notch root radius were specimen dimensions which were modified in order to achieve K_t values of 2, 3, and 6. The notch geometries were obtained from Peterson's handbook of stress concentration factors (Ref. 12) and are also shown in Fig. 17.

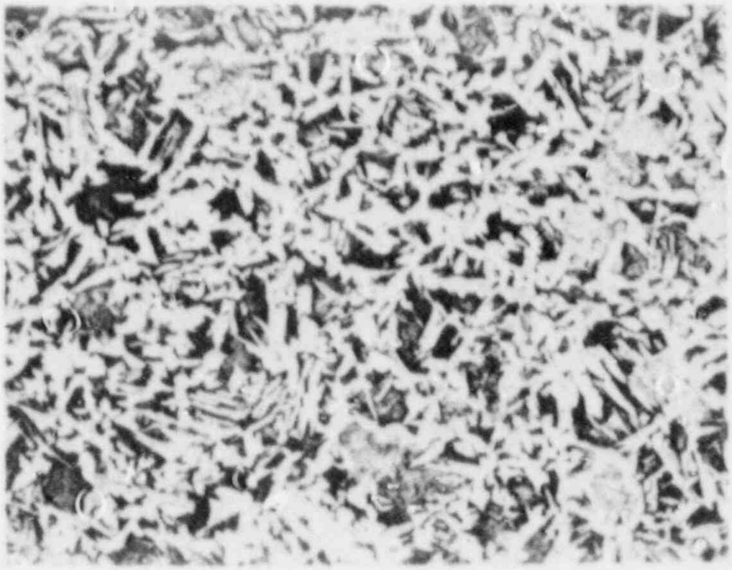

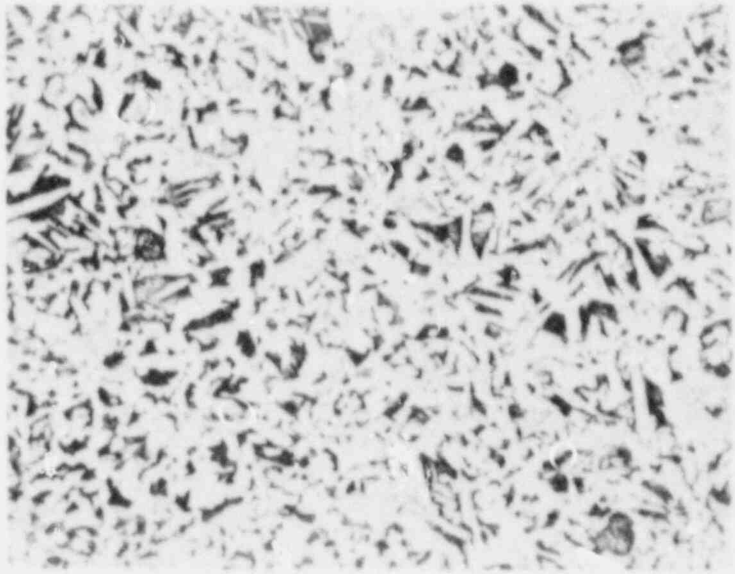

Fig. 13 Typical transverse (upper photo) and longitudinal (lower photo) cross-section microstructures of SA 106-B piping steel used in this investigation. 85x.

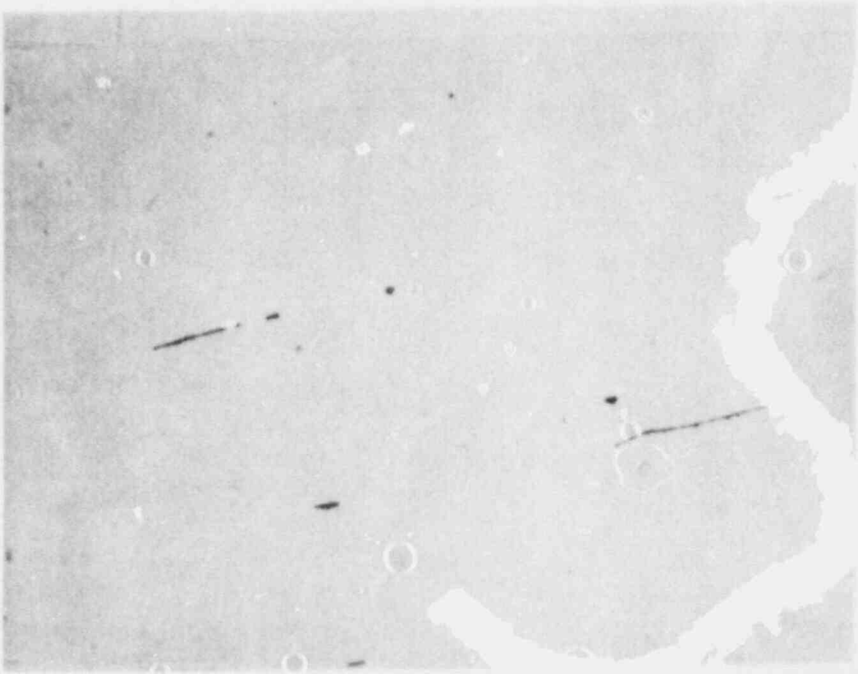

Fig. 14 Typical longitudinal cross section showing silicate inclusion distribution. 100x.

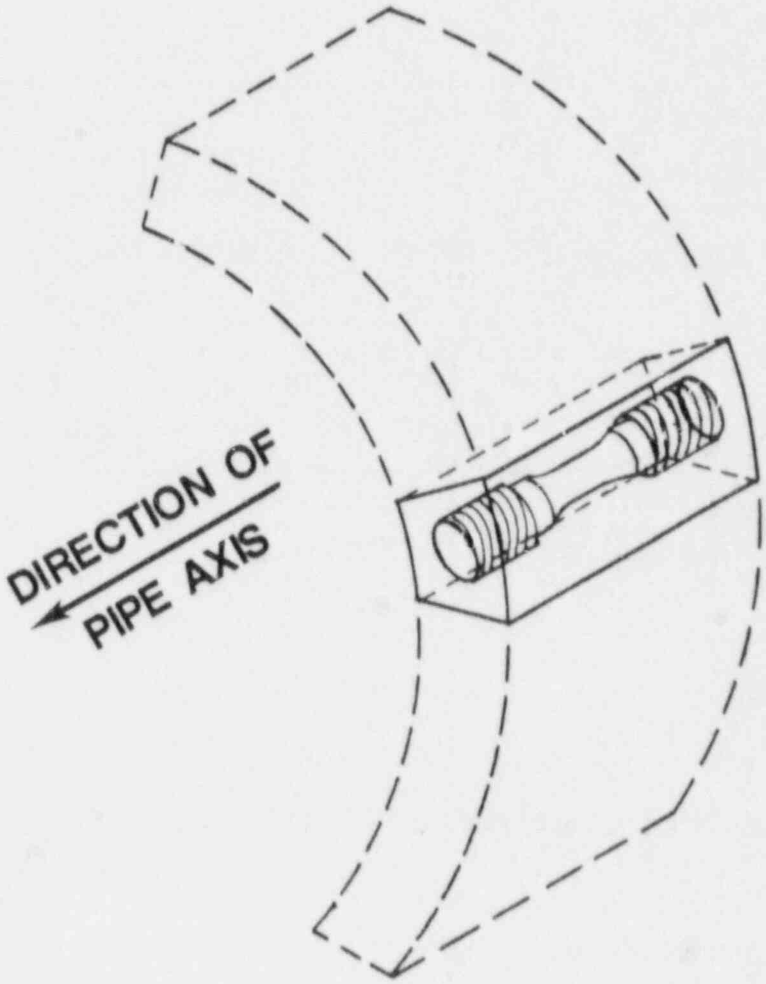

Fig. 15 Orientation of specimens used in this investigation.

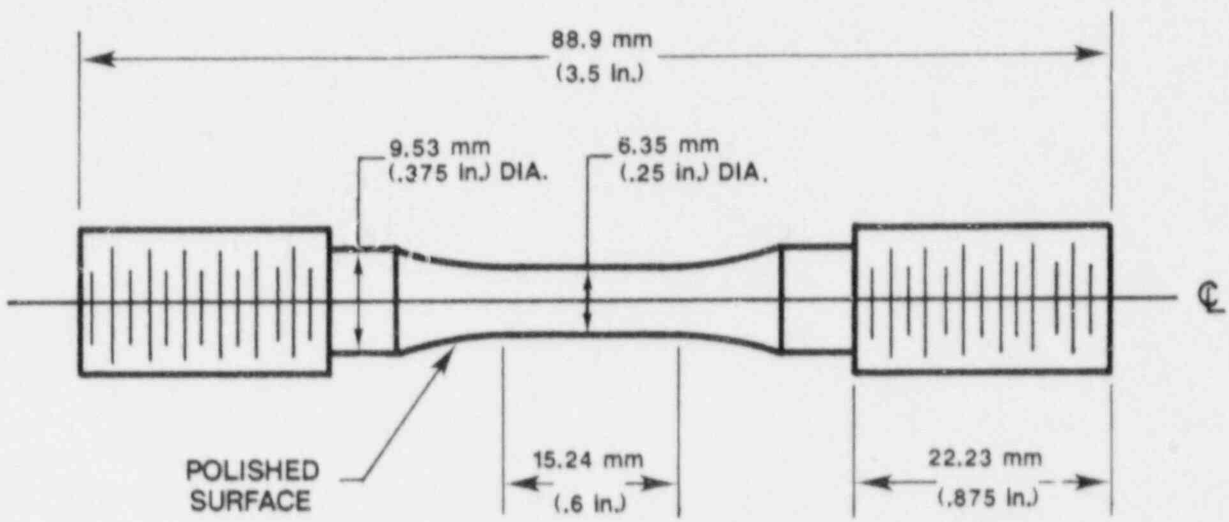

Fig. 16 Smooth specimens used in this investigation.

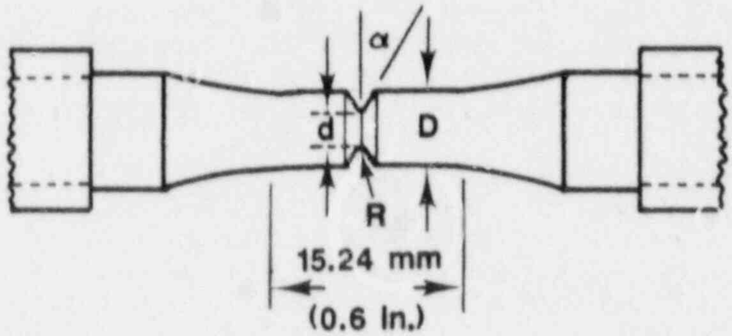

K_t	D	d	R	α (degrees)
2	8.10 mm (0.319 in.)	6.35 mm (0.250 in.)	.876 mm (0.0345 in.)	0
3	7.94 mm (0.3125 in.)	6.35 mm (0.250 in.)	.2845 mm (0.0112 in.)	0
6	9.53 mm (0.375 in.)	6.35 mm (0.250 in.)	.0711 mm (0.0028 in.)	30

Fig. 17 Geometries of notched specimens used in this investigation.

The test system consisted of a servocontrolled electrohydraulic testing system having a loading capacity of ± 44.5 kN (± 10,000 lb). The frame was of a four-post design and was situated in a horizontal configuration (Fig. 18). Even though the four-post design helped to reduce the amount of compressive buckling, it was found early in the testing program that additional stiffness of the load train was required. Therefore, a linear bearing and plate system was incorporated into the test frame (Fig. 18). This modification greatly reduced the incidence of compressive buckling of test specimens when large cyclic loads were applied. The remainder of the load train components were sufficiently thick so as to contribute negligibly to buckling.

Load-deflection histories were obtained in either of two ways. Axial strain feedback was acquired through the use of a clip gage attached to the gage section of specimens tested at room temperature, and a remotely-mounted clip gage provided axial deflection data for specimens tested at 288°C (550°F). It has been previously shown (Ref. 10) that plastic deflection (υ_p) measurements acquired with a remotely-mounted clip gage can be directly correlated with plastic strain (ε_p) measurements simultaneously acquired with a clip gage mounted on the gage length of a smooth axial specimen. An experimentally-established plot of $\Delta\upsilon_p$ vs. $\Delta\varepsilon_p$ was then constructed for room temperature tests (Fig. 19), which provided the most convenient means to determine plastic, and hence, total strains for smooth specimen fatigue tests conducted in 288°C air. Elastic strain amplitudes were estimated by the following formula:

$$\varepsilon_{ea} \approx e_{ea} = \frac{1}{2} \frac{P_{max} - P_{min}}{A_n E} \qquad (21)$$

where P_{max} and P_{min} are the maximum and minimum specimen loads, respectively, and A_n is the net cross-sectional area of the specimen.

Once ε_{ea} and ε_{pa} were estimated for each test, the total strain amplitude (ε_{ea}) was determined simply by summing ε_{ea} and ε_{pa}.

The load and deflection signals were fed into a chart recorder. Typically, hysteresis loops for the first five cycles were recorded as well as the tenth, one-hundredth, and so forth until the approximate half-life of the specimen was reached (Fig. 20).

Baseline curves for 24°C (76°F) air and 288°C air were determined for load ratio (R) = -1 tests. Notched specimens having K_t values of 2, 3, and 6 were tested for R = -1. Tests were usually started while in axial deflection control. Once the plastic strains had stabilized, the tests were switched to axial load control and were run at higher frequencies (2 to 10 Hz) until failure had occurred. In these tests, failure was considered to be the point when the crack had progressed completely through the cross section of the specimen.

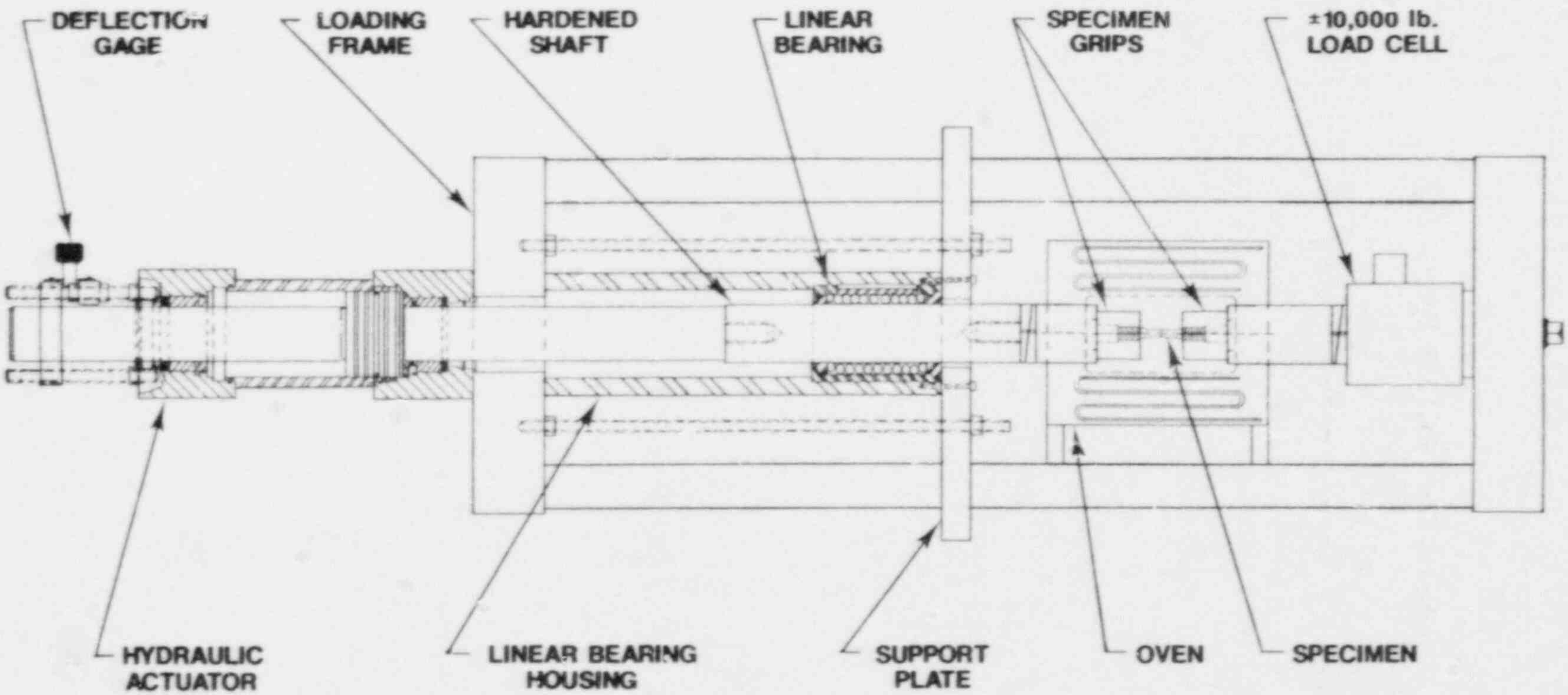

Fig. 18 Testing machine with detail of linear bearing and support plate used to stiffen the load train.

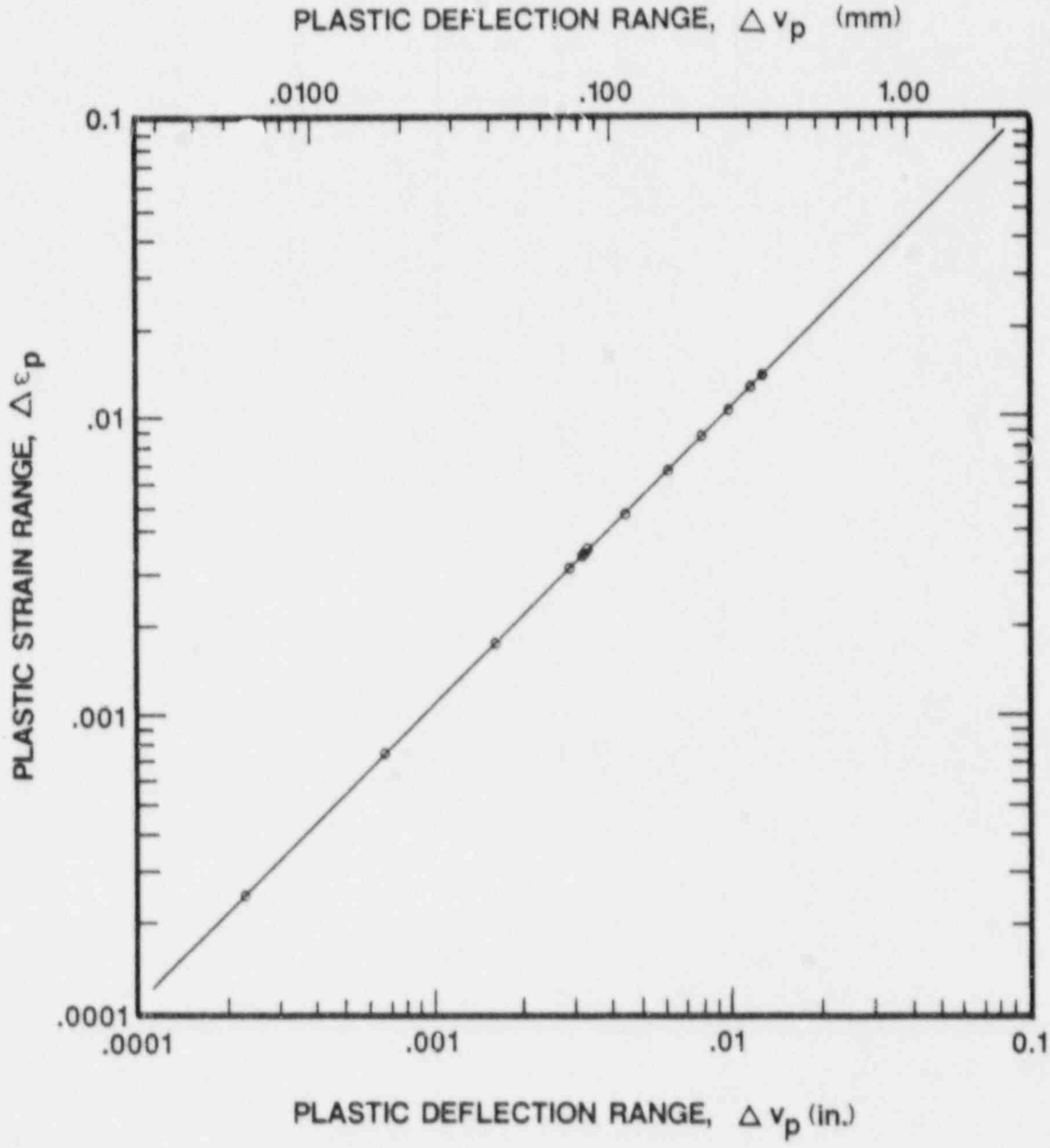

Fig. 19 Load train deflection range vs. specimen plastic strain range correlation used to determine specimen gage length total strain amplitudes.

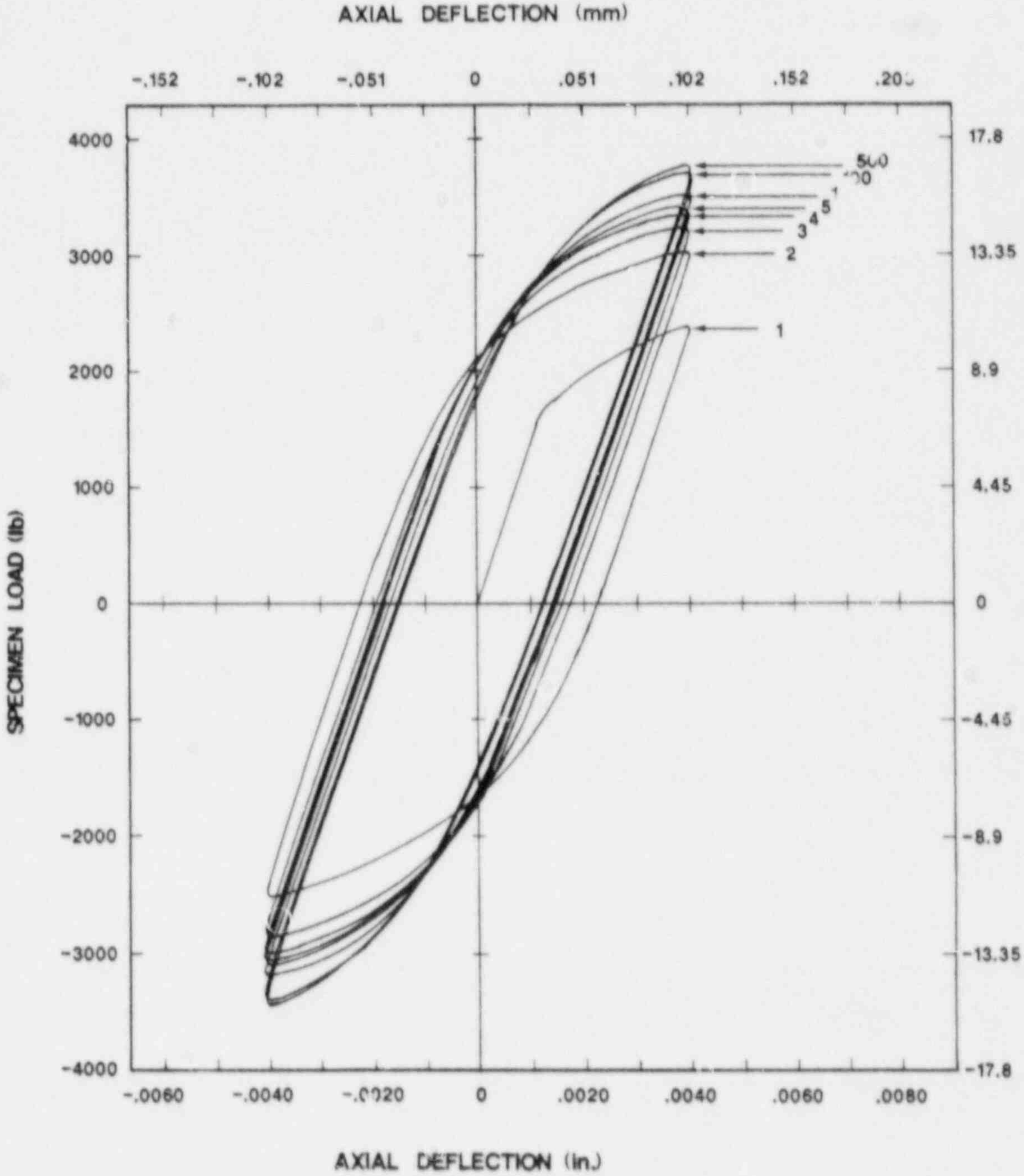

Fig. 20 Set of hysteresis loops obtained from a smooth specimen tested at 288°C (550°F).

Determination of Notch Stresses and Strains

Part of the objective of this study was to assess notch stresses and strains using different interpretations of Neuber's rule that involve the use of K_t and K_f, uniaxial and plane strain cyclic stress-strain relations, and modifications to Neuber's rule that account for net section plasticity. Notch stresses and strains were determined in the following manners:

(a) Use of K_t in Neuber's rule in conjunction with the uniaxial cyclic stress-strain law:

$$\sigma_a \varepsilon_a = \frac{(K_t S_a)^2}{E} \tag{5}$$

$$\varepsilon_a = \frac{\sigma_a}{E} + \left(\frac{\sigma_a}{A}\right)^{1/n} \tag{9}$$

(b) Use of K_t in Neuber's rule in conjunction with the plane strain cyclic stress-strain law:

$$\sigma_{1a} \varepsilon_{1a} = \frac{(K_t S_a)^2}{E_1} \tag{22}$$

$$\varepsilon'_{1a} = \frac{\sigma'_{1a}}{E'_1} + \left(\frac{\sigma'_{1a}}{A'}\right)^{1/n'} \tag{10}$$

where

$$E'_1 = \frac{E}{1 - \nu^2} \tag{11}$$

$$\sigma'_{1a} = \frac{\sigma_a}{1 - \nu + \nu^2} \tag{13}$$

$$\varepsilon'_{1a} = \frac{\varepsilon_a (1 - \nu^2)}{\sqrt{1 - \nu + \nu^2}} \tag{14}$$

$$\nu = \frac{\nu_e + \frac{E\varepsilon_{pa}}{2\sigma_a}}{1 + \frac{E\varepsilon_{pa}}{\sigma_a}} \qquad (12)$$

c) Use of K_f in Neuber's rule in conjunction with the uniaxial cyclic stress-strain law:

$$\sigma_a \varepsilon_a = \frac{(K_f S_a)^2}{E} \qquad (23)$$

$$\varepsilon_a = \frac{\sigma_a}{E} + \left(\frac{\sigma_a}{A}\right)^{1/n} \qquad (9)$$

d) Use of K_f in Neuber's rule modified for net section plasticity in conjunction with the uniaxial cyclic stress-strain law:

$$\sigma_a \varepsilon_a = \frac{K_f^2 S_a S_p e_a^*}{\sigma_y} \qquad (24)$$

$$\varepsilon_a = \frac{\sigma_a}{E} + \left(\frac{\sigma_a}{A}\right)^{1/n} \qquad (9)$$

where

$$e_a^* = \frac{S_a^*}{E} + \left(\frac{S_a^*}{A}\right)^{1/n} \qquad (25)$$

$$S_a^* = S_a \frac{\sigma_y}{S_p} \qquad (20)$$

$$S_p = 0.36 \frac{1}{1 - \frac{2a}{D}} + 0.91 \quad \sigma_y \qquad (26)$$

The equation for S_p (stress at fully plastic limit load) was modified f.om an expression for fully plastic limit load (Ref. 33).

4. RESULTS AND DISCUSSION

4.1 Smooth Specimen Tests

Cyclic stress-strain curves were constructed for SA 106-B steel at both 24°C (76°F) and 288°C (550°F) from incremental step tests conducted at the approximate half-life of each specimen. Both curves are plotted in Fig. 21. Equations for uniaxial cyclic stress-strain for both temperatures were fitted to each curve. The equation for 24°C is:

$$\varepsilon_a = \frac{\sigma_a}{205,810} + \left(\frac{\sigma_a}{689.68}\right)^{1/0.13739} \quad (27)$$

where σ_a is in MPa,

or

$$\varepsilon_a = \frac{\sigma_a}{29.85 \times 10^6} + \left(\frac{\sigma_a}{105,425}\right)^{1/0.13739}$$

where σ_a is in psi.

The equation for uniaxial cyclic stress-strain at 288°C is:

$$\varepsilon_a = \frac{\sigma_a}{190,780} + \left(\frac{\sigma_a}{747.33}\right)^{1/0.08661} \quad (28)$$

where σ_a is in MPa,

or

$$\varepsilon_a = \frac{\sigma_a}{27.67 \times 10^6} + \left(\frac{\sigma_a}{115,935}\right)^{1/0.08661}$$

where σ_a is in psi. Table 3 contains cyclic stress-strain properties of SA 106-B steel at both 24°C and 288°C.

SA 106-B steel was found to exhibit higher values for cyclic stress at 288°C than at 24°C. This behavior is believed to be attributed to dynamic strain aging effects commonly found in many low carbon steels (Ref. 34). In order for strain aging effects to occur, there must be a sufficient quantity of carbon and/or other interstitial solute atoms such as nitrogen in solution. As the metal is cycled, dislocation structures are formed. Low amplitude cycling produces isolated dislocation cloud structures that contain a large proportion of small loops from heavily-jogged screw dislocations, whereas high amplitude

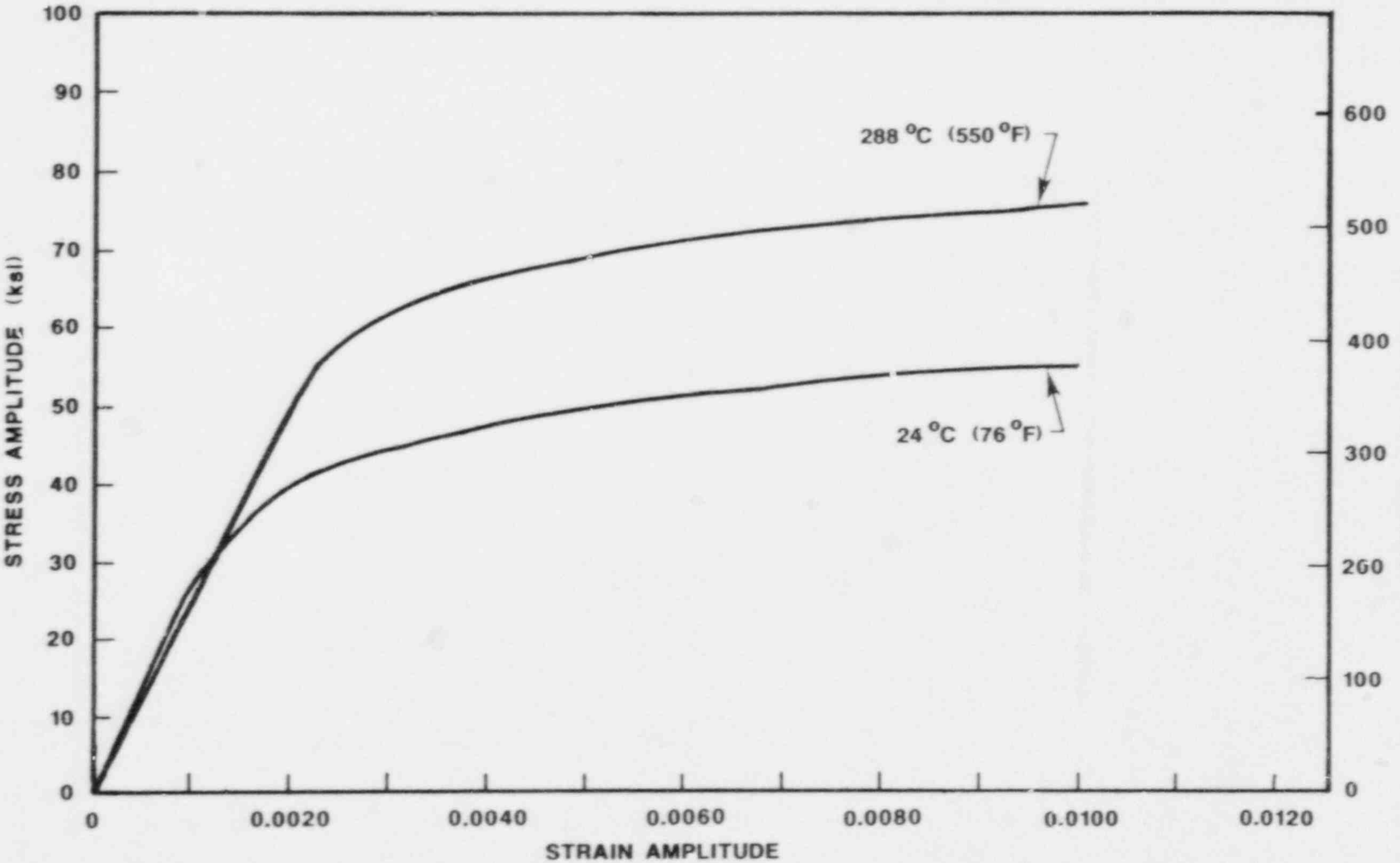

Fig. 21 Cyclic stress-strain curves for SA 106-B steel at 24°C (76°F) and at 288°C (550°F).

cycling produces dislocation cell structures (Ref. 35). When in solution, carbon tends to capture and lock low amplitude dislocations, causing dislocation loop clouds to become very dense. Therefore, the hardness of the material increases which is reflected by the increase in cyclic flow stress. The interaction of dynamic strain aging of persistant slip bands (PSB's) results in the alteration of fatigue strength, which will be discussed in a later section.

Table 3 Cyclic Stress-Strain Properties of SA 106-B Steel at 24°C and 288°C. Properties Were Measured at the Approximate Half-Life of Each Test Specimen. Waveform: Triangular. R = -1.00. Frequency: 0.50 Hz.

Temperature		Elastic Modulus		Yield Stress (0.002 Offset)		Stress at 0.010 Total Strain	
(°C)	(°F)	(MPa)	(ksi)	(MPa)	(ksi)	(MPa)	(ksi)
24	76	205,810	29,850	319.9	46.4	375.8	54.5
288	550	190,780	27,670	462.0	67.0	522.0	75.7

Fatigue tests were conducted on smooth specimens at 24°C and 288°C under reversed (R = -1) loading conditions. The results are shown in Figs. 22, 23. Tables 4 and 5 contain the data in tabular form. Figure 22 plots strain amplitude as a function of cycles to failure while Fig. 23 plots pseudostress amplitudes according to ASME Sec. III procedures (Ref. 25). The Coffin-Manson strain-life equation was fitted to the strain-life curves by dividing the total strain into elastic and plastic components. The strain-life relationship for 24°C is:

$$\epsilon_a = 0.00339\ (N_f)^{-0.08242} + 0.37010\ (N_f)^{-0.56217} \tag{29}$$

The strain-life relationship for 288°C is:

$$\epsilon_a = 0.00477\ (N_f)^{-0.08450} + 0.45487\ (N_f)^{-0.71029} \tag{30}$$

Both of these curves are plotted on Fig. 22. The pseudotress-life curves were obtained simply by multiplying the strain-life equations by the elastic modulus. Figure 23 also contains the ASME Sec. III carbon steel mean data line and the ASME design curve.

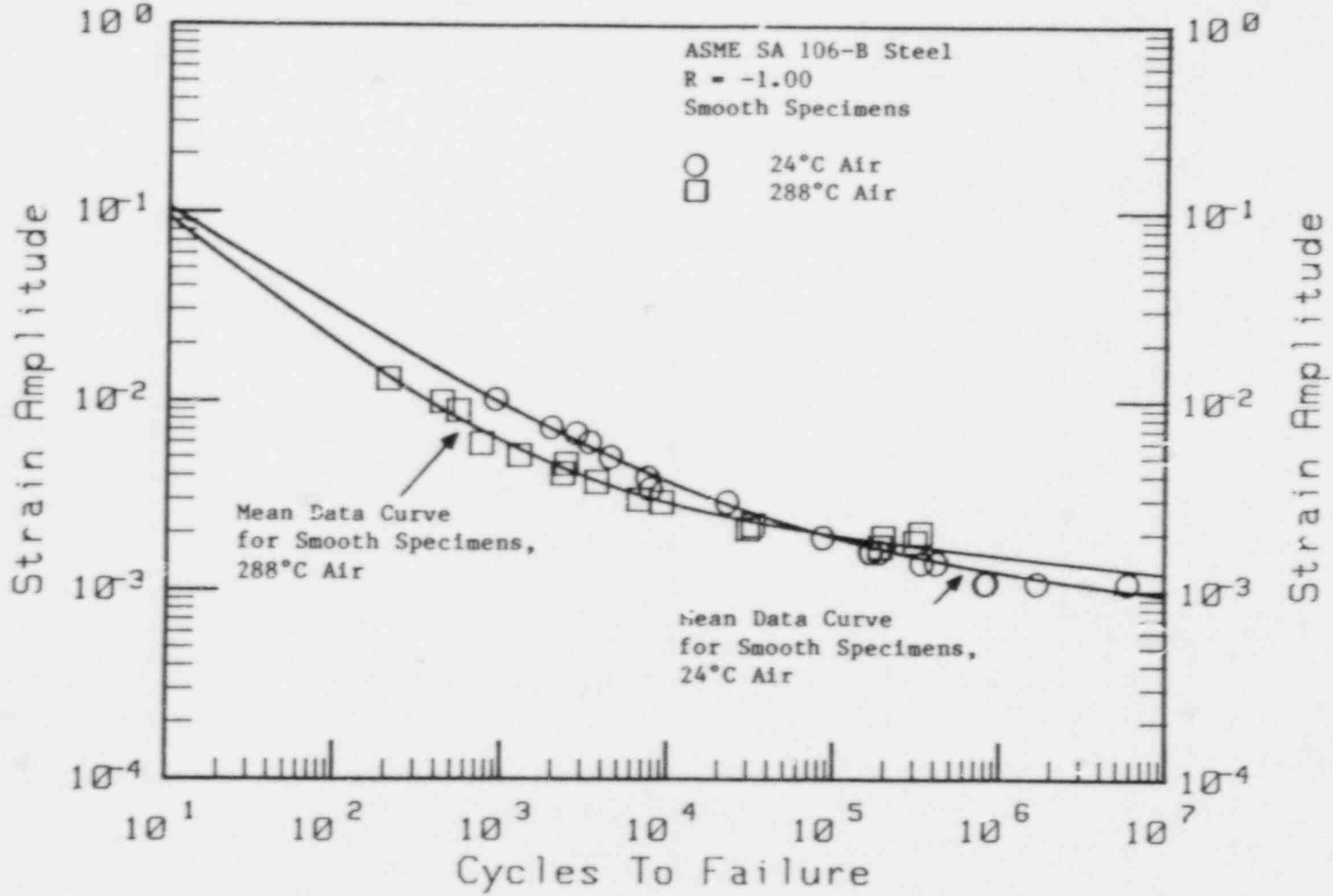

Fig. 22 Strain-life plots for smooth specimens of SA 106-B steel in air at 24°C (76°F) and at 288°C (550°F).

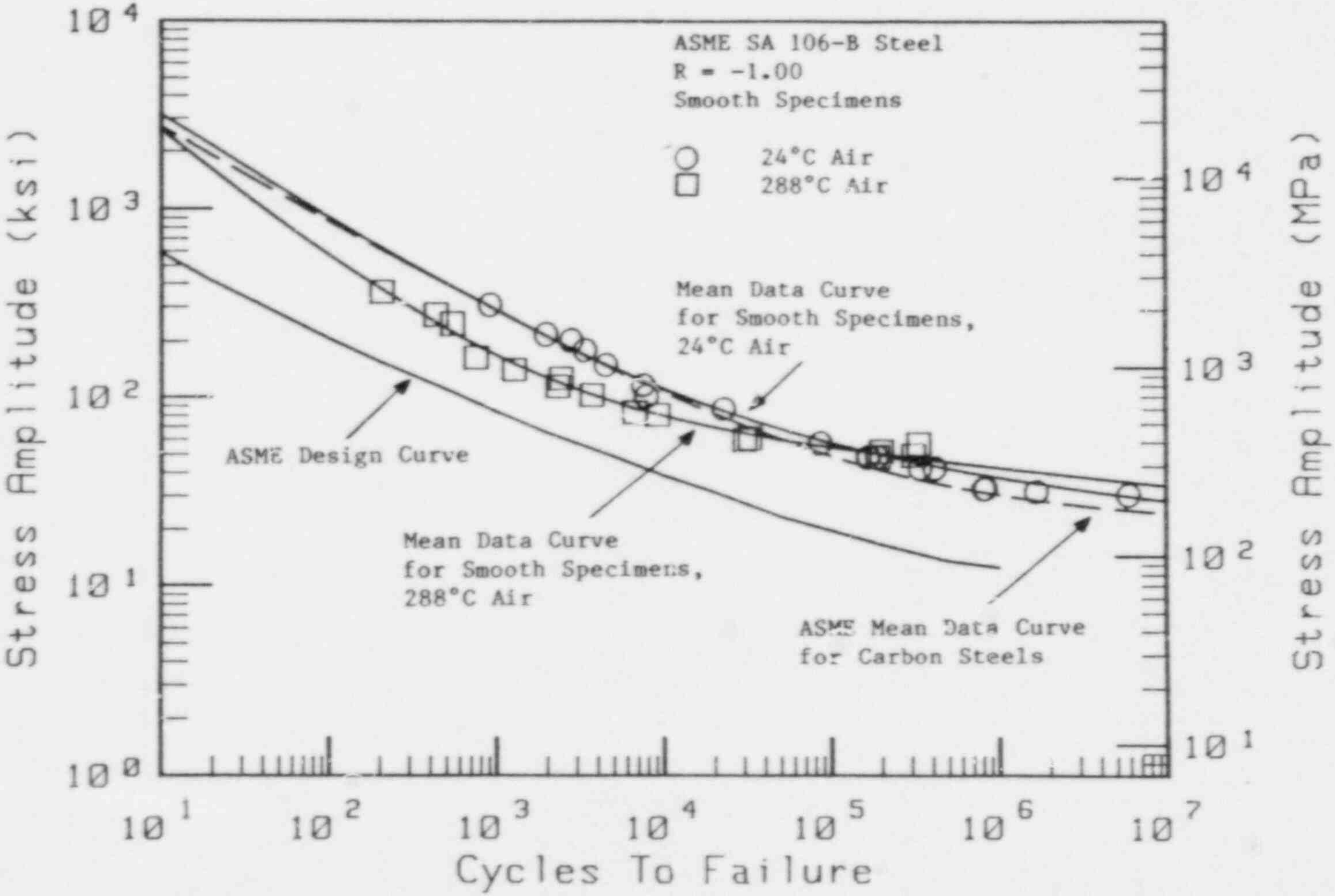

Fig. 23 ASME Code pseudostress-life plots for smooth specimens of SA 106-B steel in air at 24°C (76°F) and at 288°C (550°F). Figure also shows the ASME design curve and ASME mean data curve for carbon steels.

Table 4 Fatigue Life Data For Smooth Specimens of SA 106-B Steel tested in 24°C (76°F) Air at 1.0 Hz and R = -1.00; Elastic Modulus: 205.8 x 10^3 MPa (29.85 x 10^6 psi).

Specimen	Net Section Stress Amplitude (MPa)	Net Section Stress Amplitude (ksi)	Strain Amplitude	Pseudostress Amplitude (MPa)	Pseudostress Amplitude (ksi)	Cycles to Failure
ZP11-48	365	52.9	0.0060	1235	179.1	3,315
ZP11-138	418	63.6	0.0102	2099	304.5	900
ZP11-13	305	44.3	0.0034	700	101.5	7,720
ZP11-145	380	55.1	0.0067	1389	201.4	2,740
ZP11-8	236	34.2	0.0014	288	41.8	337,040
ZP11-10	225	32.7	0.0011	225	32.7	824,190
ZP11-23	236	34.2	0.0014	288	41.8	411,780
ZP11-30	218	31.6	0.0011	218	31.6	1.656 x 10^6
ZP11-31	24	34.9	0.0019	391	56.7	85,200
ZP11-37	31	46.1	0.0039	803	116.4	7,370
ZP11-39	241	30.6	0.0011	211	30.6	5.88 X 10^6
ZP11-43	279	40.5	0.0029	597	86.6	22,470
ZP11-22	225	32.7	0.0011	225	32.7	806,060
ZP11-82	401	58.1	0.0072	1491	216.3	1,940
ZP11-4	246	35.7	0.0016	330	47.8	187,340
ZP11-15	246	35.7	0.0016	330	47.8	164,980
ZP11-51	309	44.8	0.0016	330	47.8	166,800

Table 5 Fatigue Life Data For Smooth Specimens of SA 106-B Steel tested in 288°C (550°F) Air at 1.0 Hz and R = -1.00; Elastic Modulus: 109.8×10^3 MPa (27.67×10^6 psi).

Specimen	Net Section Stress Amplitude (MPa)	Net Section Stress Amplitude (ksi)	Strain Amplitude	Pseudostress Amplitude (MPa)	Pseudostress Amplitude (ksi)	Cycles to Failure
ZP11-17	468	67.8	0.0041	782	113.4	2,300
ZP11-109	538	78.1	0.0089	1698	246.3	540
ZP11-70	443	64.3	0.0037	706	102.4	3,670
ZP11-14	356	51.6	0.0021	401	58.1	30,200
ZP11-56	424	61.5	0.0029	553	80.2	9,100
ZP11-28	463	67.1	0.0046	878	127.3	2,400
ZP11-11	427	62.0	0.0030	572	83.0	6,600
ZP11-21	492	71.4	0.0059	1126	163.3	745
ZP11-60	525	76.2	0.0051	973	141.1	1,260
ZP11-74	375	54.4	0.0022	420	60.9	32,370
ZP11-9	329	47.7	0.0018	343	49.8	308,800
ZP11-133	536	77.7	0.0099	1888	273.9	430
ZP11-131	591	85.7	0.0130	2480	359.7	205

The most striking feature in Figs. 22 and 23 is the difference in slope of the curves at each test temperature. At high strain amplitudes, the 288°C data exhibit lower lives to failure than do specimens tested at 24°C. However, specimens tested at strain amplitudes smaller than roughly 2×10^{-3} exhibited the opposite effect. At 10^7 cycles, SA 106-B exhibited a fatigue strength of 232 MPa (33.7 ksi) at 288°C and a fatigue strength of 185 MPa (26.8 ksi) at 24°C. It is believed that the enhancement of high cycle fatigue strength at PWR environment temperatures is due to dynamic strain aging effects.

Fatigue strength effects from dynamic strain aging depend on events occurring within the regions of active slip (PSB's) since, during fatigue cycling, almost all of the applied strain is accomodated by dislocation movement within the PSB's (Ref. 36). If strain aging is weak or nonexistent, slip bands at the metal surface have been observed to broaden with progressive cycling (Ref. 37). When strain aging effects are large, dislocation locking by dissolved carbon atoms in the regions of high dislocation density (outside the PSB's) further increases the dislocation density within the PSB walls. The PSB's then become narrow and sharply defined. As a consequence, slip activity becomes highly localized and the local plastic strains within these areas increase in magnitude. Crack nucleation susceptibility within the narrowed PSB's is therefore enhanced.

However, the mobile dislocations remaining within the PSB's must be constrained in order to cause enhancement in fatigue strength (Ref. 38). This is accomplished by the formation of stable carbides within PSB's. Carbon tends to form carbides with iron, manganese, and nitrogen when the reaction kinetics are favorable. When plain carbon steels are cooled rapidly from the austenitic temperature range much of the carbon is trapped in solution and is available for carbide formation. Strain aging has been found to occur at temperatures ranging from just above room temperature to over 400°C (752°F) (Refs. 39, 40). This temperature range facilitates mass transfer of carbon atoms either by diffusion from one interstitial site to the next, or by "pipe" diffusion through dislocation atmospheres (Ref. 37). The resulting carbides can range in size, distribution, and degree of coherency with the matrix, depending on the thermal treatment and aging time. Interaction of cyclic strains with the carbides inside the PSB's is critical to dislocation slip activity modification. When high amplitude dislocation movement prevails, mobile screw dislocations within the PSB's shear apart the continually forming carbides, causing much of the available carbon to remain in solution, thereby resulting in little or no increase in fatigue strength. The level of fatigue strength observed in SA 106-B steel for strain amplitudes greater than 2×10^{-3} is consistent with this mechanism.

The interaction of PSB carbides with low amplitude dislocation movement is more complex. Fatigue strength enhancement due to strain aging results when a uniform dispersion of the smallest noncoherent carbides that resist dislocation shearing is formed (Ref. 37). The amount of plasticity within the sharply defined PSB's is suppressed when dislocation motion is thus restricted. Studies performed by

Wilson, et al. (Ref. 39) on 0.45% carbon steel have shown that specimens aged and fatigued at 130°C (266°F) and 165°C (330°F) exhibited enhanced fatigue limits. The surface of his test samples showed evidence of diffuse slip with little evidence of strain concentrations within isolated slip bands or of microcracking. Conversely, specimens that were aged and fatigued at 60°C (130°F) showed no increase in fatigue strength; narrow slip bands containing many microcracks were observed. The specimens fatigue-aged at the higher temperature contained noncoherent precipitates within the PSB's whereas the specimens fatigue-aged at the lower temperature exhibited dispersions of small, coherent, and unstable carbides which did not resist dislocation shearing.

Our observation of enhanced fatigue strength of SA 106-B steel fatigued at PWR environment temperatures is consistent with the incoherent carbide model of dynamic strain-aging. At high strain amplitudes, screw dislocations within the PSB's undergo large amplitude dislocation movements and continually shear apart at the nucleating carbides and force carbon back into solution. As a result, SA 106-B steel exhibits no apparent enhancement in fatigue strength for high strain amplitude tests conducted at 288°C (Figs. 22, 23). On the other hand, low amplitude screw dislocation movement within PSB's do not carry enough energy to shear apart the incoherent carbides, and the amount of plastic strain carried by PSB's is restricted. The result is an increase in fatigue strength observed at 288°C for low strain amplitudes (Figs. 22, 23). Li and Leslie (Ref. 40) showed a similar effect on the fatigue strength of AISI 1020 steel as shown in Fig. 24.

The reduction in low cycle fatigue strength of SA 106-B steel smooth specimens at 288°C results in nonconservative positioning of the ASME Section III design curve for carbon steel in the low cycle regime. The design curve was intended to provide a margin of safety from unseen deleterious effects that could arise from variables such as environment, surface finish, material variability, residual stresses, size effects, and statistical scatter of data. This was to be accomplished by providing design safety factors of 2 on stress or 20 on life, whichever is greater. The results in this investigation have clearly shown that the design curve for carbon steels is less conservative in terms of the results of 288°C air environment smooth specimen R = -1 tests, and therefore significantly reduces the margin of safety in the low cycle regime. Based on the results of this investigation to date, a revised Section III design curve for carbon steels could be positioned below the current design curve as shown in Fig. 25. This figure suggests that a revised design curve would more adequately impose the margin of safety as characterized by the 2 and 20 reduction factors for stress or number of cycles, and may be justifiable solely on the basis of temperature (and hence, dynamic strain aging) effects observed in SA 106-B piping steel. However, a Code revision such as this should be based on (1) an experimental data base generated from a test matrix that would encompass variables such as type of piping steel, variations in composition within each specification, and test temperature and (2) PWR environment test results, some of which are currently being conducted under the current program.

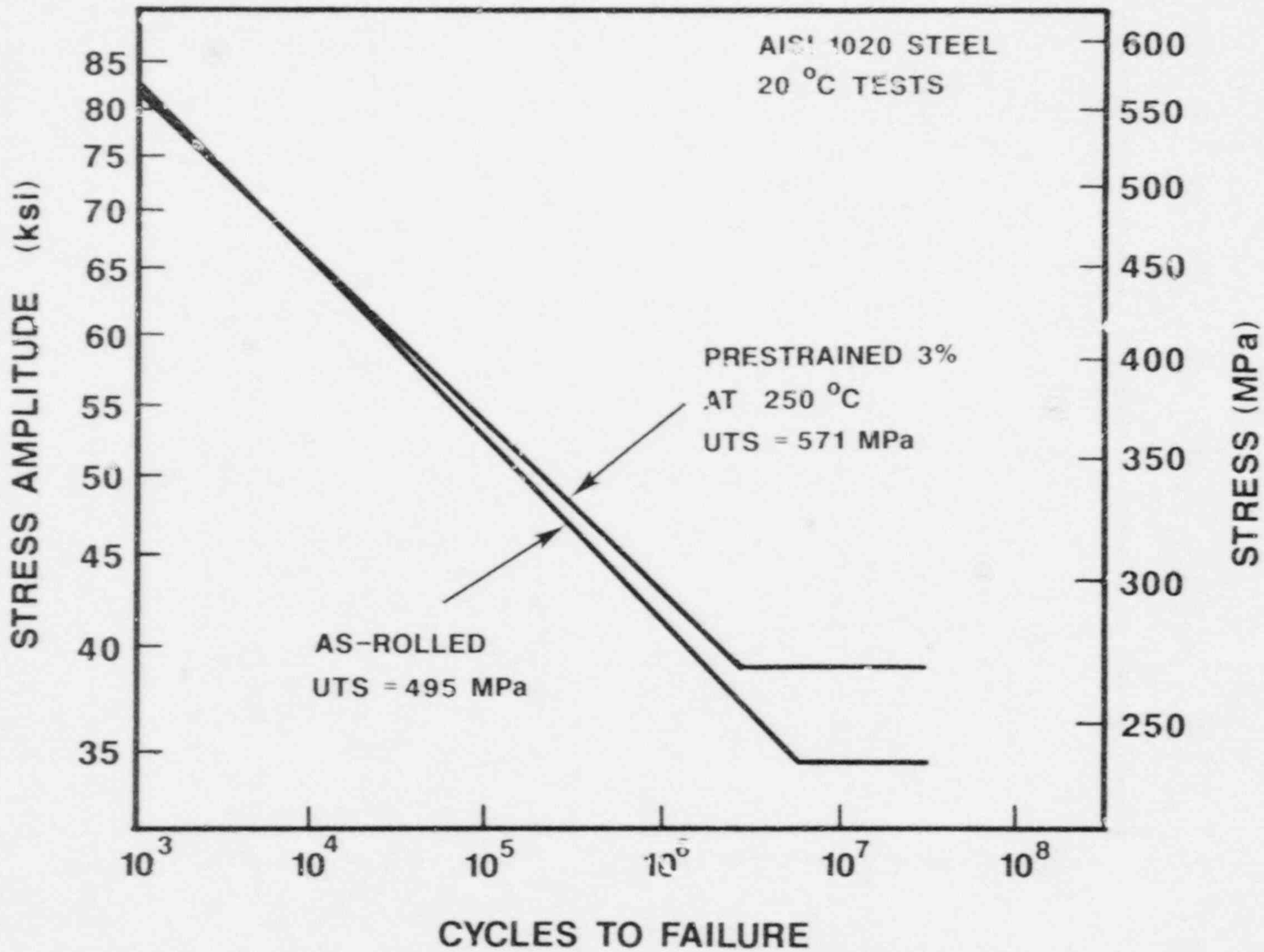

Fig. 24 Stress-life plots of AISI 1020 steel showing the effect of strain aging on fatigue strength (Ref. 40).

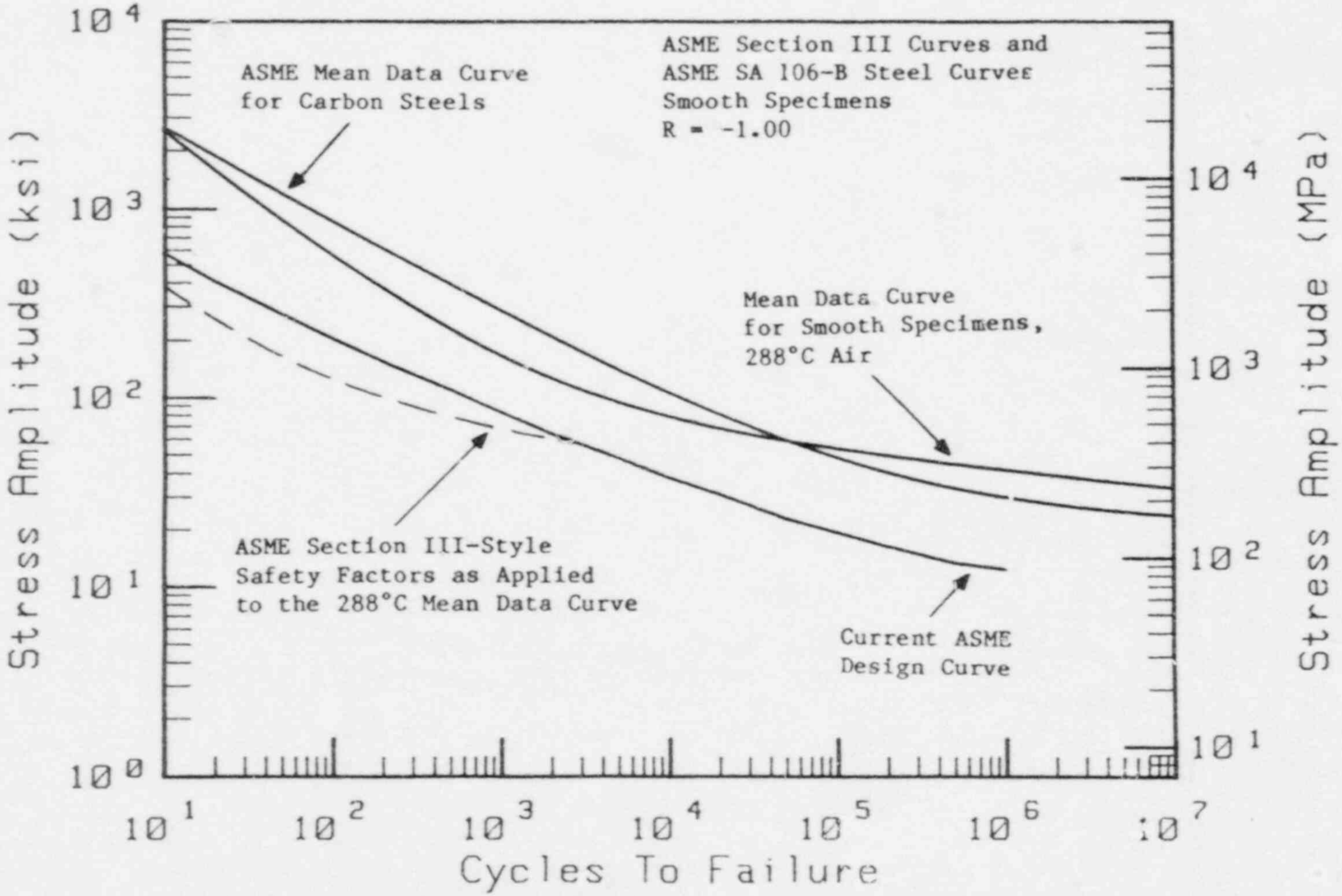

Fig. 25 Dotted line represents ASME Section III-style safety factors as applied to the mean data curve of SA 106-B steel smooth specimens tested in 288°C (550°F) air.

4.2 Notched Specimen Tests

The results for all smooth and notched specimen tests conducted at 288°C are plotted in Fig. 26 as a function of net section stress amplitude vs. cycles to failure. Table 6 contains the data points in tabular form. As expected, a reduction in cycles to failure was observed in the notched specimens at longer lives. The notch effect appears to decrease with increasing net section stress amplitude until no more notch effect is observed at stress amplitudes that correspond to lives shorter than 10^3 cycles. This phenomenon has previously been observed in ductile steels (Ref. 41).

The value for baseline notch factor (K_f) can be determined for 10^7 cycles simply as the ratio of smooth specimen fatigue strength to notched specimen fatigue strength. These values are also shown in Table 5. At higher K_t values, the empirically-determined values for K_f are considerably less then K_t, owing to the ductile nature of SA 106-B steel.

4.3 Neuber Analysis

Interpretation of the notched specimen data using different versions of the Neuber formula which included K_t or K_f, use of the Neuber formula in conjunction with either the plane stress or plane strain cyclic stress-strain equation, and a plasticity-modified Neuber relation are presented in Figs. 27, 28, and 29. Tables 7 - 10 contain the data points in tabular form. These figures plot notch root strain amplitudes obtained from each Neuber variation vs. cycles to failure for each notch root geometry. The results according to each analysis method are discussed below:

(a) Use of K_t in Neuber's rule in conjunction with the uniaxial cyclic stress-strain law: The results for K_t = 2 data correlate well with the smooth specimen data but the K_t = 3 and K_t = 6 data yield strain amplitudes which are larger than those of smooth specimen data. The K_t = 6 data predicts strain amplitudes which fall significantly above the fatigue curve generated from smooth specimens. This method of analysis yielded the most conservative results of all methods.

(b) Use of K_t in Neuber's rule in conjunction with the plane strain cyclic stress-strain law: Again, the results for the K_t = 2 data correlate well with the smooth specimen data. The K_t = 3 data fell above the smooth specimen data. Data of K_t = 6 yielded strain amplitudes much higher in value than strain amplitudes from the smooth specimens. This method yielded results which were less conservative than the method in (a) above. The use of the cyclic stress-strain curve corrected for plane strain conditions was expected to improve the data correlation but did not. Similar corrections for plane strain conditions in notched specimens yielded better results for other investigators (Ref. 10, 31).

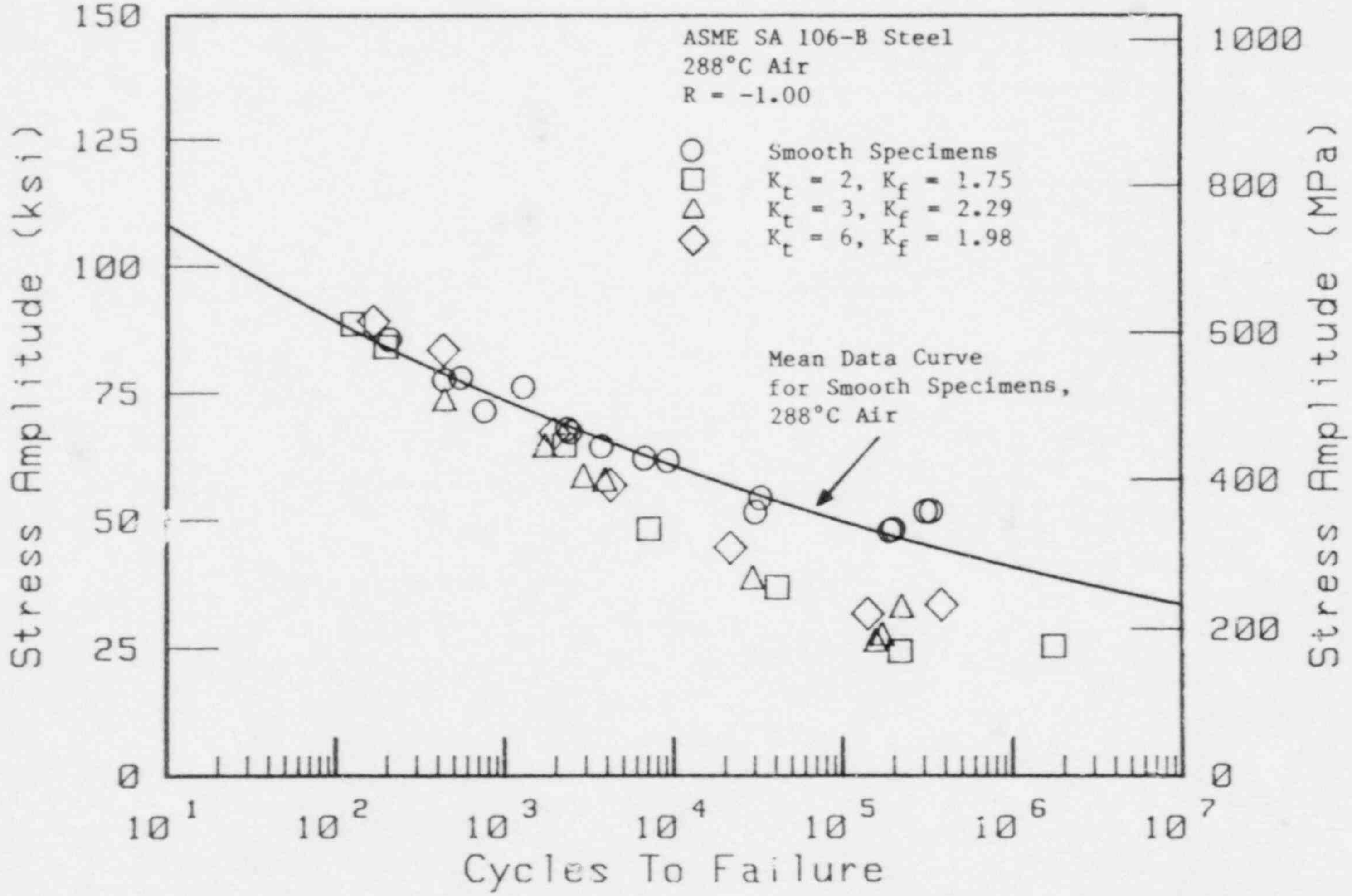

Fig. 26 Net section stress-life plots of both smooth and notched SA 106-B steel specimens in 288°C (550°F) air.

Table 6 Notched Specimen Life Data For ASME SA 106-B Steel Tested in 288°C (550°F) Air at a Frequency of 1.0 Hz and at a Load Ratio of -1.00. Net Section Stress Amplitude Values

Specimen	K_t	K_f	Net Section Stress Amplitude (MPa)	Net Section Stress Amplitude (ksi)	Cycles to Failure
K2-1	2	1.75	462	67.0	1,930
K2-2	2	1.75	577	83.7	425
K2-3	2	1.75	614	89.1	165
K2-4	2	1.75	307	44.5	21,510
K2-5	2	1.75	392	56.9	4,170
K2-7	2	1.75	232	33.6	380,970
K2-9	2	1.75	219	31.8	140,380
K3-1	3	2.29	193	28.0	171,010
K3-2	3	2.29	268	38.8	29,200
K3-3	3	2.29	400	58.0	3,860
K3-5	3	2.29	445	64.5	1,695
K3-22	3	2.29	411	59.6	2,880
K3-7	3	2.29	230	33.3	222,550
K3-10	3	2.29	510	74.0	435
K3-15	3	2.29	184	26.7	156,610
K6-1	6	1.98	254	36.9	40,825
K6-3	6	1.98	170	24.7	218,300
K6-2	6	1.98	334	48.4	7,070
K6-5	6	1.98	445	64.6	2,220
K6-6	6	1.98	613	88.9	125
K6-14	6	1.98	176	25.5	1,740,500
K6-18	6	1.98	580	84.1	195

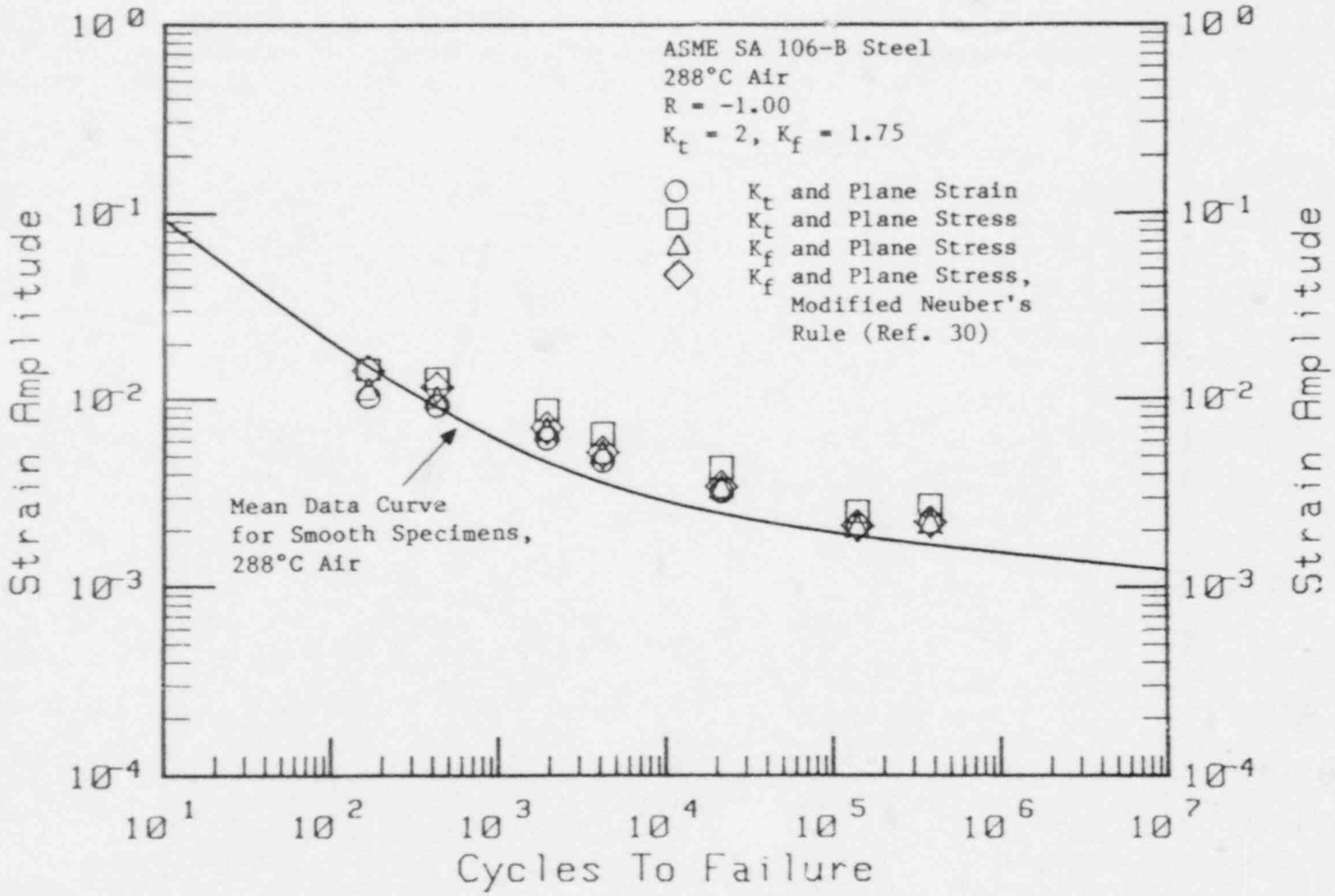

Fig. 27 Strain-life plots of K_t = 2 (K_f = 1.75) SA 106-B steel specimens in which notch strain amplitudes were estimated using four different variations of Neuber's rule.

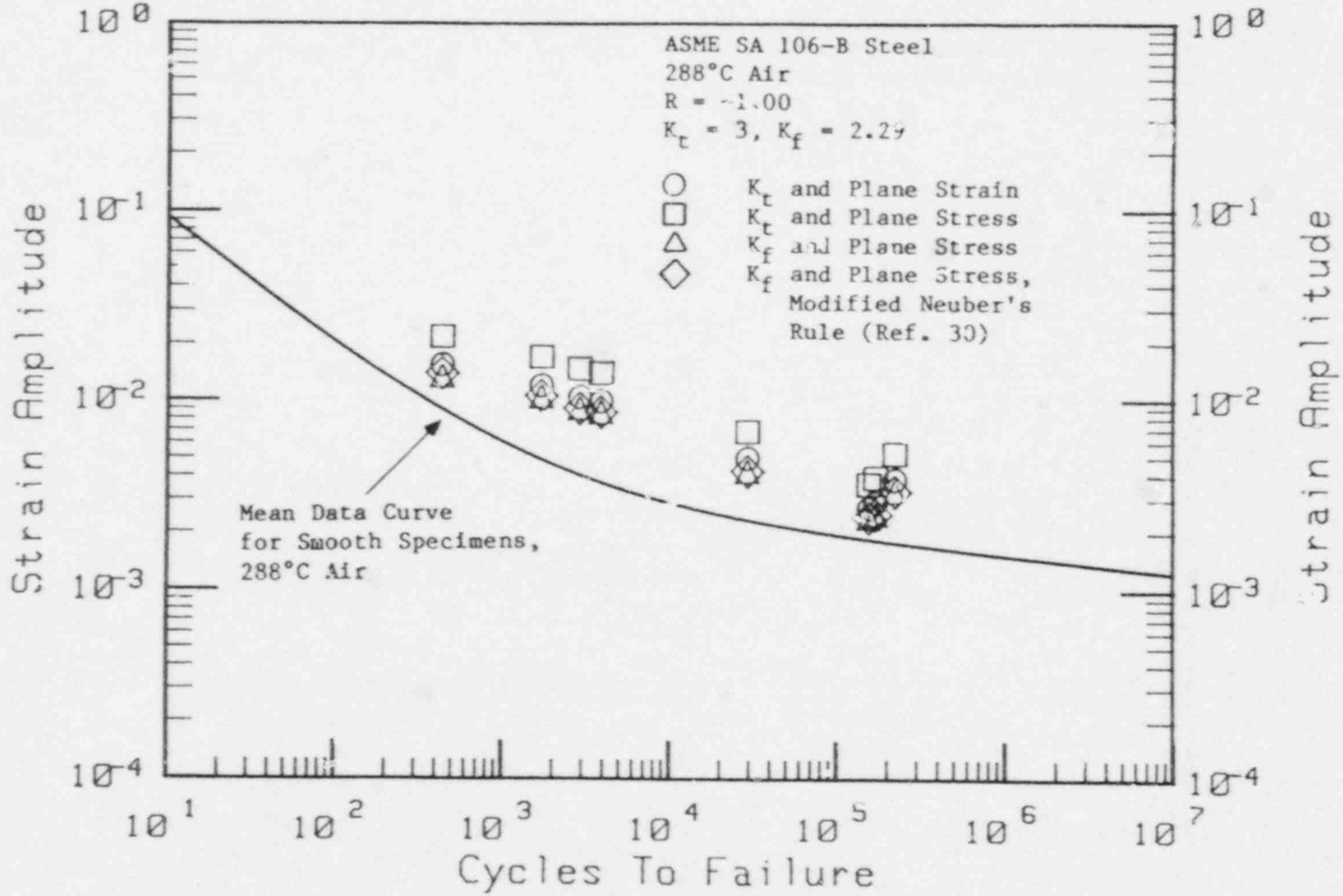

Fig. 28 Strain-life plots of K_t = 3 (K_f = 2.29) SA 106-B steel specimens in which notch strain amplitudes were estimated using four different variations of Neuber's rule.

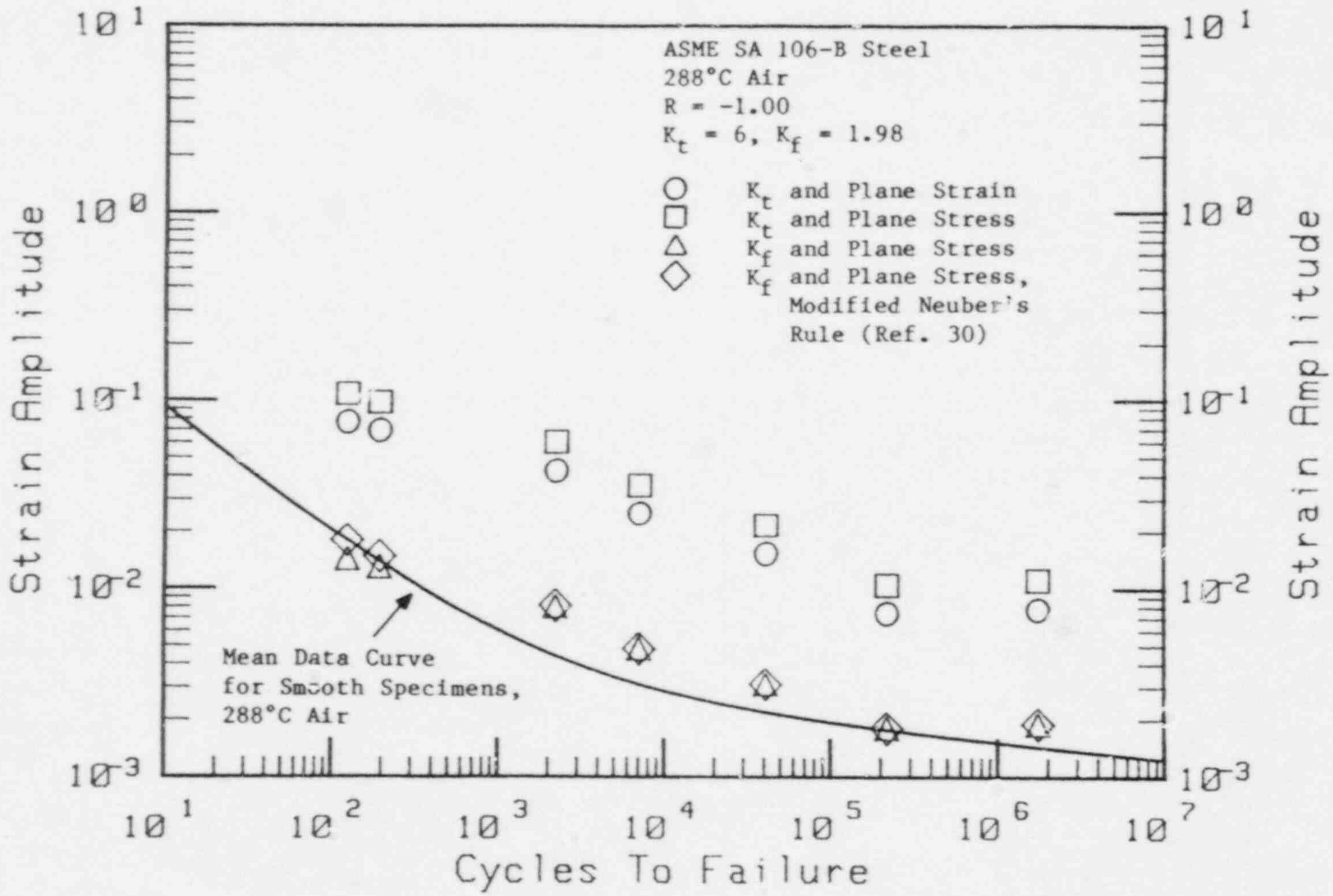

Fig. 29 Strain-life plots of K_t = 6 (K_f = 1.98) SA 106-B steel specimens in which notch strain amplitudes were estimated using four different variations of Neuber's rule.

Table 7 Fatigue Analysis of Notched Specimen Data (see Table 4). Notch Analysis Was Accomplished by Using K_t in Neuber's Rule in Conjunction With the Plane Strain Cyclic Stress-Strain Curve

Specimen	K_t	K_f	Notch Stress Amplitude (MPa)	Notch Stress Amplitude (ksi)	Notch Strain Amplitude	Pseudostress Amplitude (MPa)	Pseudostress Amplitude (ksi)	Cycles to Failure
K2-1	2	1.75	657	95.3	0.0062	1,300	188.5	1,930
K2-2	2	1.75	692	100.3	0.0092	2,050	279.3	425
K2-3	2	1.75	701	101.6	0.0103	2,154	312.4	165
K2-4	2	1.75	566	82.1	0.0032	665	96.4	21,510
K2-5	2	1.75	627	90.9	0.0047	982	142.4	4,170
K2-7	2	1.75	460	66.7	0.0022	467	67.7	380,970
K2-9	2	1.75	436	63.3	0.0021	441	63.9	140,380
K3-1	3	2.29	548	79.5	0.0029	612	88.8	171,010
K3-2	3	2.29	632	91.6	0.0049	1,020	147.9	29,200
K3-3	3	2.29	697	101.1	0.0098	2,064	299.3	3,860
K3-5	3	2.29	712	103.3	0.0119	499	362.4	1,695
K3-22	3	2.29	701	101.7	0.0103	2,168	314.4	2,880
K3-7	3	2.29	598	86.7	0.0038	794	115.1	222,550
K3-10	3	2.29	731	106.0	0.0153	3,205	464.9	435
K3-15	3	2.29	532	77.1	0.0027	574	83.3	156,610
K6-1	6	1.98	730	105.9	0.0152	3,190	462.7	40,825
K6-3	6	1.98	674	97.7	0.0074	1,551	224.9	218,300
K6-2	6	1.98	766	111.1	0.0250	5,234	769.2	7,070
K6-5	6	1.98	803	116.4	0.0424	8,897	1290.4	2,220
K6-6	6	1.98	844	122.4	0.0765	16,031	2325.1	125
K6-14	6	1.98	674	98.4	0.0078	1,641	238.0	1,740,500
K6-18	6	1.98	836	121.3	0.0690	14,470	2098.7	195

Table 8 Fatigue Analysis of Notched Specimen Data (see Table 4). Notch Analysis Was Accomplished by Using K_t in Neuber's Rule in Conjunction With the Uniaxial Cyclic Stress-Strain Curve

Specimen	K_t	K_f	Notch Stress Amplitude (MPa)	Notch Stress Amplitude (ksi)	Notch Strain Amplitude	Pseudostress Amplitude (MPa)	Pseudostress Amplitude (ksi)	Cycles to Failure
K2-1	2	1.75	514	74.5	0.0087	1,662	241.1	1,930
K2-2	2	1.75	537	77.9	0.0130	2,479	359.6	425
K2-3	2	1.75	544	78.9	0.0146	2,776	402.6	165
K2-4	2	1.75	463	67.2	0.0043	813	117.9	21,510
K2-5	2	1.75	495	71.8	0.0065	1,245	180.5	4,170
K2-7	2	1.75	416	60.3	0.0027	516	74.9	380,970
K2-9	2	1.75	404	58.6	0.0025	476	69.0	140,380
K3-1	3	2.29	455	66.0	0.0039	738	107.0	171,010
K3-2	3	2.29	498	72.2	0.0068	1,270	187.8	29,200
K3-3	3	2.29	541	78.5	0.0139	2,659	385.6	3,860
K3-5	3	2.29	552	80.1	0.0169	3,223	467.4	1,695
K3-22	3	2.29	544	78.9	0.0146	2,792	405.0	2,880
K3-7	3	2.29	478	69.4	0.0052	991	143.7	222,550
K3-10	3	2.29	567	82.2	0.0217	4,136	599.9	435
K3-15	3	2.29	447	64.9	0.0036	682	98.9	156,610
K6-1	6	1.98	566	82.1	0.0216	4,116	597.0	40,825
K6-3	6	1.98	525	76.1	0.0104	1,991	288.8	218,300
K6-2	6	1.98	594	86.1	0.0354	6,751	979.2	7,070
K6-5	6	1.98	623	90.4	0.0600	11,452	1661.0	2,220
K6-6	6	1.98	657	95.3	0.1079	20,576	2984.3	125
K6-14	6	1.98	528	76.6	0.0111	2,108	305.8	1,740,500
K7-18	6	1.98	652	94.5	0.0974	18,582	2695.1	195

Table 9 Fatigue Analysis of Notched Specimen Data (see Table 4). Notch Analysis Was Accomplished by Using K_f in Neuber's Rule in Conjunction With the Uniaxial Cyclic Stress-Strain Curve

Specimen	K_t	K_f	Notch Stress Amplitude (MPa)	Notch Stress Amplitude (ksi)	Notch Strain Amplitude	Pseudostress Amplitude (MPa)	Pseudostress Amplitude (ksi)	Cycles to Failure
K2-1	2	1.75	498	72.3	0.0069	1,311	190.2	1,930
K2-2	2	1.75	523	75.9	0.0102	1,950	282.8	425
K2-3	2	1.75	530	76.8	0.0114	2,182	316.4	165
K2-4	2	1.75	443	64.2	0.0034	651	94.4	21,510
K2-5	2	1.75	478	69.4	0.0052	981	142.3	4,170
K2-7	2	1.75	385	55.9	0.0022	426	61.8	380,970
K2-9	2	1.75	371	53.8	0.0021	397	57.6	140,380
K3-1	3	2.29	406	58.9	0.0025	482	69.9	171,010
K3-2	3	2.29	463	67.1	0.0042	811	117.6	29,200
K3-3	3	2.29	512	74.3	0.0086	1,636	237.3	3,860
K3-5	3	2.29	524	76.0	0.0104	1,960	287.0	1,695
K3-22	3	2.29	516	74.8	0.0090	1,717	249.1	2,880
K3-7	3	2.29	439	63.7	0.0033	629	91.3	222,550
K3-10	3	2.29	538	78.1	0.0133	2,534	367.5	435
K3-15	3	2.29	395	57.3	0.0024	450	65.3	156,610
K6-1	6	1.98	432	62.6	0.0031	589	85.2	40,825
K6-3	6	1.98	333	48.3	0.0018	341	49.5	218,300
K6-2	6	1.98	474	68.7	0.0048	923	133.8	7,070
K6-5	6	1.98	508	73.7	0.0080	1,531	222.0	2,220
K6-6	6	1.98	543	78.7	0.0142	2,715	393.8	125
K6-14	6	1.98	343	49.7	0.0019	354	51.3	1,740,500
K6-18	6	1.98	543	78.8	0.0129	2,455	356.1	195

Table 10 Fatigue Analysis of Notched Specimen Data (see Table 4). Notch Analysis Was Accomplished by Using K_f in Neuber's Rule Modified for Net Section Plasticity (Ref. 30) in Conjunction with the Uniaxial Cyclic Stress Curve

Specimen	K_t	K_f	Notch Stress Amplitude (MPa)	Notch Stress Amplitude (ksi)	Notch Strain Amplitude	Pseudostress Amplitude (MPa)	Pseudostress Amplitude (ksi)	Cycles to Failure
K2-1	2	1.75	499	72.4	0.0070	1,329	192.7	1,930
K2-2	2	1.75	531	77.0	0.0116	2,215	321.3	425
K2-3	2	1.75	543	78.8	0.0144	2,754	399.5	165
K2-4	2	1.75	443	64.2	0.0034	651	94.4	21,510
K2-5	2	1.75	478	69.4	0.0052	988	143.3	4,170
K2-7	2	1.75	385	55.9	0.0022	427	61.9	380,970
K2-9	2	1.75	371	53.8	0.0021	397	57.6	140,380
K3-1	3	2.29	406	58.9	0.0025	482	69.9	171,010
K3-2	3	2.29	463	67.2	0.0042	811	117.6	29,200
K3-3	3	2.29	513	74.4	0.0086	1,641	238.0	3,860
K3-5	3	2.29	525	76.1	0.0105	1,996	289.5	1,695
K3-22	3	2.29	516	74.3	0.0090	1,724	250.1	2,880
K3-7	3	2.29	437	63.7	0.0033	629	91.3	222,550
K3-10	3	2.29	541	78.4	0.0138	2,630	381.4	435
K3-15	3	2.29	395	57.3	0.0024	450	65.3	156,610
K6-1	6	1.98	432	62.6	0.0031	587	85.2	40,825
K6-3	6	1.98	333	48.3	0.0018	341	49.5	218,300
K6-2	6	1.98	474	68.7	0.0048	923	1343.8	7,070
K6-5	6	1.98	509	73.8	0.0081	1,544	223.9	2,220
K6-6	6	1.98	556	80.6	0.0179	3,415	495.3	125
K6-14	6	1.98	343	49.7	0.0019	354	51.3	1,740,500
K6-18	6	1.98	545	79.0	0.0147	2,810	407.5	195

(c) Use of the K_f in Neuber's rule in conjunction with the uniaxial cyclic stress-strain law: These results provided the best correlation for all methods taken into consideration. However, the correlation still tended to be conservative in its estimation of notch base strain amplitudes required to cause specimen fatigue failure when compared to strain amplitudes accumulated from smooth specimen data.

(d) Use of the K_f in Neuber's rule modified for net section plasticity: Correlation for all of the notched data was quite good, but was not as good as the method in (c) above. The modification was intended to account for the change in stress at the notch tip due to the influence of constraint on the value of fully-plastic limit load. The end result was a small increase in the conservatism of notch strain values over the values generated with the use of K_f in an unmodified Neuber equation in conjunction with the uniaxial cyclic stress-strain equation.

The strain-life behavior of notched specimens subjected to reversed loading was shown to be determined most accurately by calculating notch root cyclic strains with the use of K_f in the Neuber formulation in conjunction with the uniaxial cyclic stress-strain curve. This assessment was facilitated by comparing the local cyclic strain vs. cycles to failure data for notched specimens to strain-life data acquired from smooth specimen testing as shown in Fig. 30. A key assumption to this approach is that the number of cycles necessary for crack initiation is equal for both smooth and notched specimens if the cyclic strain histories are equal for each crack initiation site. This assumption has been proven to be valid based on studies using both smooth and notched aluminum and low carbon steel plates (Ref. 31). The results of that study are shown in Fig. 8. Benefits of the use of K_f in favor of K_t proved to be most apparent for specimens having the sharpest ($K_t = 6$) notch.

Although Neuber had originally intended that K_t be used in conjunction with his rule (Ref. 3), other investigators have modified Neuber's rule to include K_f and have found good correlation between smooth and notched specimen results (Refs. 5 - 7, 26 - 29). For blunt notches and for the most notch-sensitive materials, K_f approaches K_t, and either factor could conceivably be successfully used in the Neuber formula. The results for $K_t = 2$ specimens (Figs. 28 - 30) supports this claim for the case of blunt notches. For sharp notches, K_f is always less than K_t with larger discrepancies prevailing for more ductile materials. Previous belief dictated that the discrepancy was due to material size effects (Ref. 12). However, the work of Leis, et al. (Ref. 31) has shown that this difference is due not to size effects, but to changes in the ratio of nominal to notch deformation. Small values of nominal stress are required to induce a state of plasticity at the tip of an extremely sharp notch, and previous work by Gowda, et al. (Ref. 42) suggests that the value of K_t becomes invalid for inelastic strain amplitudes.

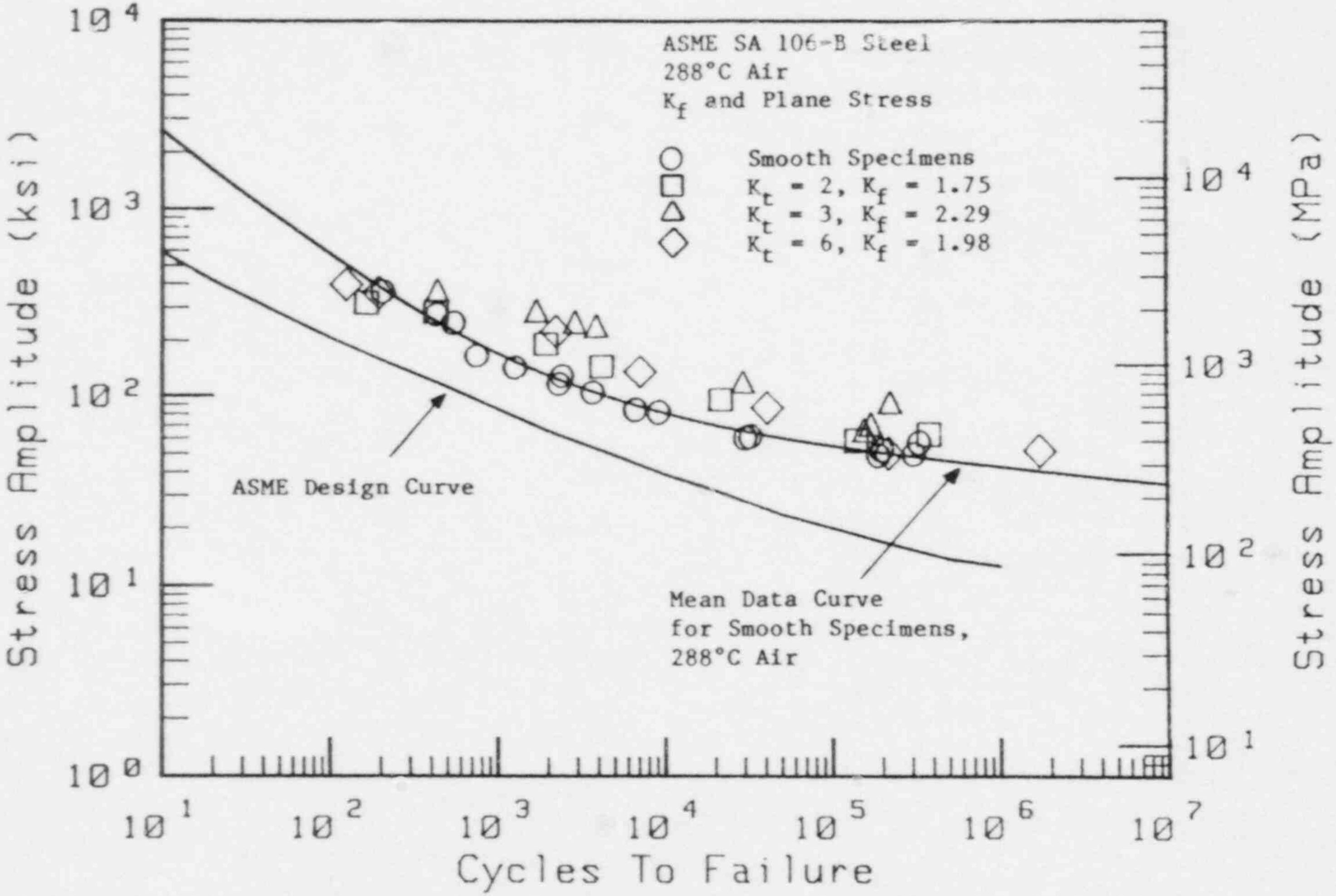

Fig. 30 ASME Code pseudostress-life plots of both smooth and notched SA 106-B steel specimens. Notch root strains, and hence, notch root pseudostresses, were estimated by using K_f in Neuber's rule in conjunction with the uniaxial cyclic stress-strain curve.

A comparison of either net section stress amplitude or corresponding Neuber-generated notch stress amplitude data with smooth specimen results quickly reveals a few fundamental differences in interpretation of their fatigue behavior (Fig. 26). Comparison of notched specimen net section stress amplitude data with smooth specimen data clearly shows the detriment of the notch on fatigue life in terms of smooth specimen stresses but fails to yield any quantitative measure of the stress state at the notch tip. The Neuber-generated notch stress amplitude data, on the other hand, tends to correlate more closely with corresponding smooth specimen stress amplitudes by providing equal indices of fatigue damage for both smooth and notched specimens. Local stress and local strain amplitudes estimated by Neuber's rule tend to most closely model the state of notch root stresses and strains using analytical formulas.

Given the capabilities and limitations of Neuber's rule, the question arises as to whether or not the results of notched specimen tests can be accurately correlated with the ASME Section III curves. As a first cut, pseudostress calculations based on notch strain estimates appear to provide a reasonable degree of correlation with smooth specimen results within an order of magnitude. However, both the inherent conservatism in Neuber's rule and the ramifications of crack propagation dominating the lives of notched specimens yields overestimations of notch stresses and strains and unfortunately does not provide the desired accuracy needed as a basis of comparison between smooth and notched specimen fatigue behavior. Once initiated, the crack grows very rapidly through the notch elastic strain field and slows down considerably once it has grown beyond the influence of the notch (Ref. 18). Such a decrease in crack growth rate could add considerably to the total number of cycles to failure and may result in increased conservatism of the data points. Once initiation has occurred, the fatigue life problem essentially becomes a fracture mechanics problem in which the use of Neuber's rule becomes very limited. Schemes which use Neuber's rule to estimate crack initiation and fracture mechanics to characterize crack propagation are probably best suited to investigate the total fatigue lives of notched specimens.

5. CONCLUSIONS

This investigation characterized the cyclic stress-strain and strain-life behavior of SA 106-B piping steel at 24°C (76°F) and at 288°C (550°F) using smooth specimens. The correlation of strain-life behavior of notched specimens with smooth specimens was facilitated by determining the most appropriate use of Neuber's rule. Therefore, the following conclusions were drawn:

- The higher value for cyclic stress amplitudes observed at 288°C from the construction of cyclic stress-strain curves at 24°C and 288°C is postulated to be due to dynamic strain aging effects.

- The fatigue limits at 10^7 cycles under completely-reversed loading for smooth specimens were estimated to be 185 MPa (26.8 ksi) at 24°C and 232 MPa (33.7 ksi) at 288°C. The observed reduction in low cycle fatigue strength at 288°C results in reduction in the safety factor of the ASME Section III design curve for carbon steels. The observed changes in fatigue strengths at PWR operating temperatures is believed to be a result of dynamic strain aging.

- Notch strain histories for blunt (K_t = 2) notches can be determined by the use of either K_t or K_f in Neuber's rule without any deviation of results.

- Notch strain histories for sharper notches (K_t = 3 and 6) are most accurately determined by the use of K_f in Neuber's rule in conjunction with the uniaxial cyclic stress-strain curve. When correlated with the results from smooth specimen tests, the data from sharply-notched specimens are conservative.

- The fatigue life curves resulting from the high temperature air environment smooth specimen results in this report provide acceptable baseline data for comparison with smooth specimen tests to be performed in PWR environments using the same type of specimens. The PWR environment test results will be used to assess the validity of the ASME Boiler and Pressure Vessel Code Section III stress-life design curves for Class 1 piping components.

- The application of Neuber's rule in the assessment of notch stress and strain amplitudes of SA 106-B steel for the purpose of fatigue life characterization results in a degree of conservatism which does not provide the accuracy needed as a basis of comparison of notched specimen results with the ASME Section III curves for carbon steels. It is concluded that schemes which use Neuber's rule to estimate crack initiation and fracture mechanics to characterize crack propagation are probably best suited as tools to investigate notched specimen total fatigue lives.

REFERENCES

1. E. Z. Stowell, "Stress and Strain Concentration at a Circular Hole in an Infinite Plate," National Advisory Committee for Aeronautics, Technical Note 2073, Apr. 1950.

2. H. F. Hardrath and L. Ohman, "A Study of Elastic and Plastic Stress Concentration Due to Notches and Fillets in Flat Plates," National Advisory Committee for Aeronautics Report 1117, 1953.

3. H. Neuber, "Theory of Stress Concentration for Shear-Strained Prismatical Bodies With Arbitray Nonlinear Stress-Strain Law," Journal of Applied Mechanics, Dec. 1961, pp. 544-550.

4. W. K. Wilson, "Elastic-Plastic Analysis of Blunt Notched CT Specimens and Applications," Journal of Pressure Vessel Technology, Vol. 96(4), Nov. 1974, pp. [illegible]3-298.

5. T. H. Topper, R. M. Wetzel, and J. Morrow, "Neuber's Rule Applied to Fatitue of Notched Specimens," Journal of Materials, JMSLA, Vol. 4(1), Mar. 1969, pp. 200-209.

6. T. H. Topper, B. I. Sandor, and J. Morrow, "Cumulative Damage Under Cyclic Strain Control," Journal of Materials, JMSLA, Vol. 4(1), Mar. 1969, pp. 189-199.

7. R. M. Wetzel, "Smooth Specimen Simulation of Fatigue Behavior of Notches," Journal of Materials, JMSLA, Vol. 3(2), Sept. 1968, pp. 646-657.

8. E. K. Walker, "Multiaxial Stress-Strain Approximations for Notch Fatigue Behavior," Journal of Testing and Evaluation, JTEVA, Vol. 5(2), Mar. 1977, pp. 106-113.

9. C. E. Jaske, H. Mindlin, and J. S. Perrin, "Cyclic Stress-Strain Behavior of Two Alloys at High Temperature," Cyclic Stress-Strain Behavior Analysis, Experimentation, and Failure Prediction, ASTM STP 519, American Society for Testing and Materials, Phila., PA, 1973, pp. 13-27.

10. N. E. Dowling, "Crack Growth During Low-Cycle Fatigue of Smooth Axial Specimens," Cyclic Stress-Strain and Plastic Deformation Aspects of Fatigue Crack Growth, ASTM STP 637, American Society for Testing and Materials, 1977, pp. 97-121.

11. N. E. Dowling, W. R. Brose, and W. K. Wilson, "Notched Member Fatigue Life Predictions by the Local Strain Approach," Fatigue Under Complex Loading - Analysis and Experiments, Society of Automotive Engineers, 1977, pp 57-84.

12. R. E. Peterson, Stress Concentration Factors, John Wiley and Sons, New York, 1974.

13. C. Visser, S. E. Gabrielse, and W. VanBuren, "A Two Dimensional Elastic-Plastic Analysis of Fracture Test Specimens," HSST Technical Report No. 4, United States Atomic Energy Commission, Oak Ridge National Laboratory, 1969.

14. J. W. Bryson and B. R. Bass, "ORMGEN.PC: A Microcomputer Program For Automatic Mesh Generation of 2-D Crack Geometries," Oak Ridge National Laboratory, USNRC Report NUREG/CR-4475, Mar. 1986.

15. J. W. Bryson, "ORVIRT.PC (Version 2.0): A 2-D Finite-Element Fracture Analysis Program for a Microcomputer," Oak Ridge National Laboratory, USNRC Report NUREG/CR-4367, July 1986.

16. C. Inversini and J. W. Bryson, "ORPLOT.PC: A Graphic Utility for ORMGEN.PC and ORVIRT.PC," Oak Ridge National Laboratory, USNRC Report NUREG/CR-4633, June 1986.

17. T. R. Leax, N. E. Dowling, W. R. Brose, and M. G. Peck, "Methodology For Correlating Fatigue Data Obtained Under Different Test Conditions," Journal for Testing and Evaluation, JTEVA, Vol. 13(6), Nov. 1985, pp. 393-404.

18. N. E. Dowling, "Notched Member Fatigue Life Predictions Combining Crack Initiation and Propagation," Fatigue of Engineering Materials and Structures, Vol. 2, 1979, pp. 129-138.

19. D. F. Socie, N. E. Dowling, and P. Kurath, "Fatigue Life Estimation of Notched Members," Fracture Mechanics: Fifteenth Symposium, ASTM STP 833, American Society for Testing and Materials, Phila., PA, 1984, pp. 284-299.

20. P. Kurath, Z. Khan, and D. F. Socie, Fatigue Life Estimation of Notched Members on a Corrosive Environment," Journal of Pressure Vessel Technology, Trans ASME, Vol. 109, Feb. 1987, pp. 135-141.

21. T. A. Prater and L. F. Coffin, "The Use of Notched Compact-Type Specimens for Crack Initiation Design Rules in High-Temperature Water Environments," Corrosion Fatigue: Mechanics Metallurgy, Electrochemistry, and Engineering, ASTM STP 801, American Society for Testing and Materials, Phila, PA, 1983, pp. 423-444.

22. T. A. Prater and L. F. Coffin, "Notch Fatigue Crack Initiation in High Temperature Water Environments: Experiments and Life Prediction," Journal of Pressure Vessel Technology, Trans ASME, Vol. 109, Feb. 1987, pp. 124-134.

23. A. R. Jack and A. T. Price, "The Initiation of Fatigue Cracks from Notches in Mild Steel Plates," International Journal of Fracture Mechanics, Vol. 6, 1970, pp. 401-409.

24. J. M. Barsom and R. C. McNicol, "Effect of Stress Concentration on Fatigue-Crack Initiation in HY-130 Steel," Fracture Toughness and Slow-Stable Cracking, ASTM STP 559, American Society for Testing and Materials, 1974, pp. 183-204.

25. ASME Boiler and Pressure Vessel Code, Nuclear Power Plant Components, Section III, Division 1, Subsection NB, Class 1 Components, American Society of Mechanical Engineers, New York, issued annually.

26. D. F. Socie, "Fatigue-life Prediction Using Local Stress-Strain Concepts," Experimental Mechanics, Vol. 17(2), Feb. 1977, pp. 50-56.

27. A. Baus, H. P. Lieurade, G. Sanz, and M. Truchon, "Correlation Between the Fatigue-Crack Initiation at the Root of a Notch and Low Cycle Fatigue Data," Flaw Growth and Fracture, ASTM STP 631, American Society for Testing and Materials, 1977, pp. 96-111.

28. P. S. Maiya, "Effects of Notches on Crack Initiation in Low Cycle Fatigue," Materials Science and Engineering, Vol. 38, 1979, pp. 289-294.

29. K. Saanouni and C. Bathias, "Study of Fatigue Crack Initiation in the Vicinity of Notches," Engineering Fracture Mechanics, Vol. 16(5), 1982, pp. 695-706.

30. T. Seeger and P. Heuler, "Generalized Applications of Neuber's Rule," Journal of Testing and Evaluation, JTEVA, Vol. 8(4), July 1980, pp. 199-204.

31. B. N. Leis, C. V. B. Gowda, and T. H. Topper, "Cyclic Inelastic Deformation and the Fatigue Notch Factor," Cyclic Stress-Strain Behavior - Analysis, Experimentation, and Failure Predictions, ASTM STP 519, American Society for Testing and Materials, Phila., PA, 1973, pp. 133-150.

32. "Standard Recommended Practice for Constant-Amplitude Low-Cycle Fatigue Testing, Designation E606-80," Annual Book of ASTM Standards, Metals - Mechanical Testing, Vol. 03.01, revised annually, American Society for Testing and Materials, Phila., PA, 1985, pp. 681-698.

33. "An Engineering Approach for Elastic-Plastic Fracture Analysis," EPRI NP-1931, Project 1237-1, Electric Power Research Institute, July 1981, pp. 3-15.

34. L. F. Coffin, "The Effect of Quench Aging and Cyclic-Strain Aging on Low Carbon Steel," Journal of Basic Engineering, Trans. ASME, Vol. 87, June 1965, pp. 351-362.

35. D. V. Wilson and J. K. Tromans, "Effects of Strain Ageing on Fatigue Damage in Low-Carbon Steel," Acta Metallurgica, Vol. 18, Nov. 1970, pp. 1197-1208

36. C. Laird, "Mechanisms and Theories of Fatigue," Fatigue and Microstructure, American Society for Metals, Metals Park, OH, 1979, pp. 149-203.

37. D. V. Wilson, "Precipitation and Growth of Carbide Particles in a Cyclically Strained Low Carbon Steel," Acta Metallurgica, Vol. 21, May 1973, pp. 673-682.

38. D. V. Wilson, "Effects of Microstructure and Strain Ageing on Fatigue Crack Initiation in Steel," Metal Science, Vol. 11, Aug./Sep. 1977, pp. 321-331.

39. D. V. Wilson and B. Mintz, "Effects of Microstructural Instability on the Fatigue Behavior of Quenched and Quench-Aged Steels," Acta Metallurgica, Vol. 20, July 1972, pp. 985-995.

40. C. C. Li and W. C. Leslie, "Effects of Dynamic Strain Aging on the Subsequent Mechanical Properties of Carbon Steels," Metallurgical Transactions A, ASM-AIME, Vol. 9A, Dec. 1978, pp. 1765-1775.

41. H. O. Fuchs and R. I. Stephens, Metal Fatigue in Engineering, Wiley-Interscience, New York, 1980, p. 159.

42. C. V. B. Gowda and T. H. Topper, "Cyclic-deformation Behavior of Notched Mild-Steel Plates in Plane Stress," Experimental Mechanics, Vol. 12(8), Aug. 1972, pp. 359-367.

NRC FORM 335 (11-81)

U.S. NUCLEAR REGULATORY COMMISSION

BIBLIOGRAPHIC DATA SHEET

1. REPORT NUMBER (Assigned by DDC)
NUREG/CR-5013
MEA-2232

2. (Leave blank)

3. RECIPIENT'S ACCESSION NO.

4. TITLE AND SUBTITLE (Add Volume No., if appropriate)
Fatigue Life Characterization of Smooth and Notched Piping Steel Specimens in 288°C Air Environments

5. DATE REPORT COMPLETED

MONTH	YEAR
February	1988

DATE REPORT ISSUED

MONTH	YEAR
May	1988

6. (Leave blank)

7. AUTHOR(S)
J. B. Terrell

8. (Leave blank)

9. PERFORMING ORGANIZATION NAME AND MAILING ADDRESS (Include Zip Code)
Materials Engineering Associates, Inc.
9700-B Martin Luther King, Jr. Highway
Lanham, MD 20706-1837

10. PROJECT/TASK/WORK UNIT NO.

11. FIN NO.
B8900

12. SPONSORING ORGANIZATION NAME AND MAILING ADDRESS (Include Zip Code)
Division of Engineering
Office of Nuclear Regulatory Research
U. S. Nuclear Regulatory Commission
Washington, D. C. 20555

13. TYPE OF REPORT
Technical Report

PERIOD COVERED (Inclusive dates)

14. (Leave blank)

15. SUPPLEMENTARY NOTES

16. ABSTRACT (200 words or less)

Fatigue strain-life tests were conducted on ASME SA 106-B piping steel at 24°C (76°F) and at PWR operating temperature, 288°C (550°F), under completely reversed loading. Smooth specimens were tested at both temperatures whereas specimens containing notches of various acuities were tested at 288°C. Fatigue limits at 10^7 cycles were estimated to be 185 MPa (26.8 ksi) at 24°C and 232 MPa (33.7 ksi) at 288°C. The difference in fatigue strength observed at the PWR temperature is postulated to be due to dynamic strain aging processes. However, there is a reduction in low cycle fatigue strength at this temperature which results in a decrease in the intended safety factor of the ASME Section III design curve for carbon steels. Notch strain histories were estimated for the notched specimen tests using various interpretations of Neuber's rule. It was concluded that the use of the fatigue notch concentration factor (K_f) in the Neuber relation in conjunction with the uniaxial cyclic stress-strain curve provided the best correlation of notched specimen fatigue data with results obtained from smooth specimen tests. The notched specimen strain-life results derived from the application of Neuber's rule alone proved to be conservative when compared to smooth specimen test results to such an extent that Neuber-generated notch stress and strain amplitudes cannot be compared to the ASME Section III fatigue curves for carbon steels.

17. KEY WORDS AND DOCUMENT ANALYSIS

17a. DESCRIPTORS

Fatigue	Temperature Effects
Notch	Dynamic Strain Aging
Piping Steels	Neuber's Rule
SA 106-B Steel	Stress-Life

17b. IDENTIFIERS/OPEN-ENDED TERMS

18. AVAILABILITY STATEMENT
Unlimited

19. SECURITY CLASS (This report)
Unclassified

20. SECURITY CLASS (This page)
Unclassified

21. NO. OF PAGES

22. PRICE
$

☆U. S. GOVERNMENT PRINTING OFFICE:1988-202-292:80062

UNITED STATES
NUCLEAR REGULATORY COMMISSION
WASHINGTON, D.C. 20555

OFFICIAL BUSINESS
PENALTY FOR PRIVATE USE, $300

SPECIAL FOURTH-CLASS RATE
POSTAGE & FEES PAID
USNRC
PERMIT No. G-67

120555078877 1 1AN1RF1R5
US NRC-OARM-ADM
DIV OF PUB SVCS
POLICY & PUB MGT BR-PDR NUREG
W-537
WASHINGTON DC 20555

NUREG/CR-5013

STEEL SPECIMENS IN 288 °C AIR ENVIRONMENTS